

We are IntechOpen, the world's leading publisher of Open Access books Built by scientists, for scientists

6,900

Open access books available

186,000

International authors and editors

200M

Downloads

Our authors are among the

154

Countries delivered to

TOP 1%

most cited scientists

12.2%

Contributors from top 500 universities



WEB OF SCIENCE™

Selection of our books indexed in the Book Citation Index
in Web of Science™ Core Collection (BKCI)

Interested in publishing with us?
Contact book.department@intechopen.com

Numbers displayed above are based on latest data collected.
For more information visit www.intechopen.com



Transparent Conductive Oxide (TCO) Films for Organic Light Emissive Devices (OLEDs)

Sunyoung Sohn and Hwa-Min Kim
*Catholic University of Daegu
Republic of Korea*

1. Introduction

Transparent conducting oxide (TCO) thin films of In_2O_3 , SnO_2 , ZnO , and their mixtures have been extensively used in optoelectronic applications such as transparent electrodes in touch panels, flat panel displays (FPDs), and other future devices. The first chapter provides an introduction to the basic physics of TCO films and surveys the various topics and challenges in this field. It includes a description of the TCO materials used in some of the organic light emissive devices (OLEDs) that have been studied extensively to date, the performance of various OLEDs, and a brief outlook.

Chapter 2 focuses on TCO material development of p-type and n-type. Typical oxide kind of TCO materials consist of In_2O_3 , SnO_2 , and ZnO . These are applied as a TCO films with n-type semiconducting property according to highly doped dopants which acting as a carrier. Until today, in a n-type TCO materials, indium tin oxide (ITO) doped with SnO_2 of 10 wt.% in In_2O_3 has been widely commercialized. This is because the ITO film has high performance of both good electrical conductivity of $\sim 10^{-4} \Omega\text{-cm}$ and high transmittance of $\sim 90\%$ when the ITO film is coated on glass substrate. At present, $\text{In}_2\text{O}_3\text{-SnO}_2$ (ITO) films are most commonly used as TCO films, but they have some disadvantages, such as high cost, instability, poor surface roughness, and toxicity in their further applications. And amorphous ITO film deposited at low temperature has low resistance under moist heat, which leads to a decrease in its conductivity and light transmittance. In addition, unfortunately, the price of Indium is dramatically increasing every day due to a mix-up between the supply and demand of raw materials by the exhaustion of Indium source. On the other hand, some zinc-based TCO materials have good optical and electrical properties comparable to the ITO films, as well as low cost, high stability, excellent surface uniformity, and good etching selectivity. The zinc-based TCO films are, therefore, regarded as promising substitutes for ITO film. In Chapter 3, the Indium-based and Zinc-based TCO Materials, and their electrical, optical, and structural properties will be discussed. Particularly, since more stringent specifications for TCO films have been required for realization of both higher resolution and larger screen size of FPDs, and preparation of high-quality TCO films at low temperature is very important to realize advanced optoelectronic devices.

Chapter 4 will introduce the new TCO materials, such as: organic conductors like poly(3,4-ethylenedioxy thiophene):poly(styrenesulphonicacid) (PEDOT:PSS), and the expanding field of nanomaterials including carbon nanotubes, nanoparticles, and composite materials combining one or more of these materials. For example, long metallic nanotubes have been

found to have volume conductivities of ca. 700,000 S/cm, which is almost as conductive as pure copper. Moreover, carbon nanotubes (CNTs) because of their covalent bonding do not suffer from electromigration, which is a common problem that leads to failure in thin metal wires and films. It is the covalent bonds of CNTs that make them thermally stable and highly resistant to chemical damage. Therefore, these cheap and flexible transparent organic and nano conductors can be an appropriate substitution for conventional ITO in the next generation optoelectronic devices.

ITO films are very brittle and easily broken down by externally applied bending forces, while the ITO films are widely used as the transparent electrode for display device. Finally, Chapter 5 mainly examines how external deformation influences the mechanical stability of ITO thin films on flexible polymer substrates for flexible OLEDs (FOLEDs), typically in a bent state.

2. Classification of TCO materials

TCOs are very useful materials to transparent optoelectronics because they have unique features of optical properties in the visible light region such as the transparency over ~85% and optical band gap greater than 3 eV and controllable electrical conductivity such as carrier concentrations of at least 10^{20} cm^{-3} and resistivity of about 10^{-4} ohm cm . (Kim et al., 2011) Notwithstanding their extraordinarily wide controllable conductivity range including that of semiconductor behavior, their applications are limited to transparent electrodes. It seems to us that the origin of this limited application is due to a lack of p-type conducting transparent oxide materials. TCO materials are naturally n-type degenerate semiconductors and the lack of a high quality p-type TCO always has been the main obstacle in front of the fabrication of a fully transparent complementary metal-oxide semiconductor (CMOS)-like devices. Although n-type TCO such as ZnO, SnO₂ and ITO are key components in a variety of technologies, p-type TCO are an emerging area with little work previous to four years ago. However, realization of good TCO could significantly impact a new generation of transparent electrical contacts for p-type semiconductors and organic optoelectronic materials and in conjunction with n-type TCOs could lead to a next generation of transparent electronics.

2.1 p-type TCO

Since the first report of a p-type TCO was NiO, In 1997, there was a report of transparent p-type conducting films of CuAlO₂ showing considerable improvement over NiO. (Sato et al., 1993; Kawazoe et al., 1997) Although the conductivity of 1 S cm^{-1} was about three orders of magnitude smaller than that of n-type materials, the result was promising. Since the discovery of p-type conductivity in CuAlO₂, many Cu(I) based delafossites having transparency and p-type conductivity have been synthesized, such as CuScO₂, CuYO₂, CuInO₂, CuGaO₂, and CuCrO₂. Conductivity of the CuInO₂ film deposited under working oxygen pressure of 7.5 mTorr and 450 °C was reported as $2.8 \times 10^{-3} \text{ S/cm}$. (Roy et al., 2003) And also, the dependence of the electrical conductivity of CuInO₂ films upon the deposition temperature was investigated. With increasing deposition temperature from room temperature to 600 °C, the conductivity increases and reaches a value of $5.8 \times 10^{-2} \text{ S/cm}$ for the film deposited at 400 °C temperature. Indeed, other structures have been identified that combine p-type conductivity and optical transparency in Cu(I) based materials, including SrCu₂O₂ and layered oxychalcogenides (LaCuOS), although to date the p-type TCO with the highest conductivity is a delafossite (Mg doped CuCrO₂). Among various candidate materials, ZnO is one of the most important members of TCOs. Like the other members (e.g.: SnO₂, In₂O₃, IZO, and ITO), ZnO

have been applied. Among the candidates of shallow acceptors, nitrogen is the most tried one due to its nearest-neighbor bond length of 1.88 Å that is similar to the Zn–O bond length of 1.93 Å. The p-type ZnO have been made by nitrogen using various deposition techniques like sputtering, chemical vapor deposition (CVD), metalorganic CVD (MOCVD), pulsed laser deposition (PLD) and spray pyrolysis (SP). (Huang et al., 2010) Growing p-ZnO was an important milestone in “Transparent Electronics”, allowing fabrication of wide band gap p-n homo-junctions, which is a key structure in this field. It was anticipated that higher conductivity and optical transmission could be obtained by ZnO doped with N, F, P, Sb, and As. In this section, we discussed the necessary requirements in the electronic energy band structure and crystal structure with Cu based p-type TCO. The chemical formula of delafossites is AMO_2 in which A is the monovalent cation and M is a trivalent cation. Delafossites have a hexagonal, layered crystal structure: the layers of a cations and MO_2 are stacked alternately, perpendicular to the c-axis. As a class, p-type materials now include the copper-based delafossites $CuMO_2$.

Fig. 1 shows the schematic representation of the necessary electronic configuration of the cationic species. In this combination, considerable covalency can be expected for both the bonding and anti-bonding levels. The valence band edge shifts from the $2p$ levels of oxygen ions to the anti-bonding levels because both the cation and anion have a closed shell electronic configuration. It should be noted that the localization nature of the valence band edge is greatly reduced by the modification. Cu and Ag have the appropriate d^{10} states for this purpose. (Sheng et al., 2006)

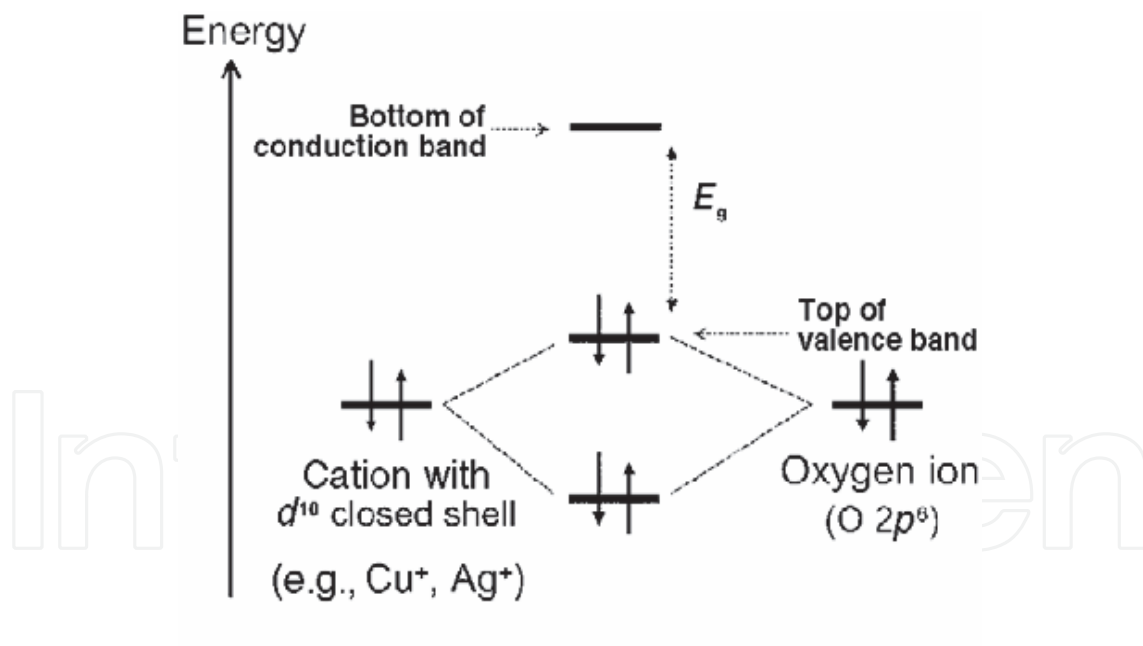


Fig. 1. Schematic of the chemical bond between an oxide ion and a cation that has a closed shell electronic configuration.

The metal states interact with some of the O $2p$ states, which push up a more dispersive band above the non-bonding O $2p$ or Cu $3d$ states. Tetrahedral coordination of oxide ions is advantageous for p-type conductivity, as it acts to reduce the localization behavior of $2p$ electrons on oxide ions. The valence state of the oxide ions can be expressed as sp^3 in this conformation. Since the Cu_2O has a rather small band gap (E_g) of 2.17 eV, we found that the

Eg of p-type TCO should be greater than 3.1 eV. Hence enlargement of the band gap would be another structural requirement for designing p-type TCOs, so that there is no absorption of visible photons. Two families of Cu based TCOs have been developed from this idea, CuMO_2 ($M = \text{Al, Ga, In, Sc, Cr, Y, B, etc.}$) with the delafossite structure and the non-delafossite structure SrCu_2O_2 , LaCuOCh ($\text{Ch} = \text{chalcogen}$). The band structural properties of these materials were calculated in detail by Nie et al., Robertson et al., and Ueda et al. (Sheng et al., 2006)

2.1.1 CuBO_2

A study by Snure and Tiwari has identified a new group 13 delafossite, CuBO_2 , as a new p-type TCO. (Snure & Tiwari, 2007) In this study, a density functional theory (DFT) study are measured, and examining the detailed electronic structure of CuBO_2 . (David et al., 2009) This group show conclusively that (i) the lattice parameters reported by Snure and Tiwari are not consistent with previous experimental trends and need to be reinvestigated, (ii) the valence band features of CuBO_2 are consistent with other delafossite p-type TCOs, (iii) the effective hole masses of the valence band maximum (VBM) are consistent with the reported good conductivity, and (iv) the predicted indirect band gap and optical band gap of CuBO_2 are 3.21 eV and ~ 5.1 eV, respectively. The GGA + U calculated bandstructure of CuBO_2 along the high symmetry lines taken from Bradley and Cracknell is shown in Fig. 2. The VBM is situated at the F point, while the conduction band minimum (CBM) lies at Γ , giving an indirect band gap of 1.94 eV, with the smallest direct band gap situated at Γ and measuring 3.21 eV.

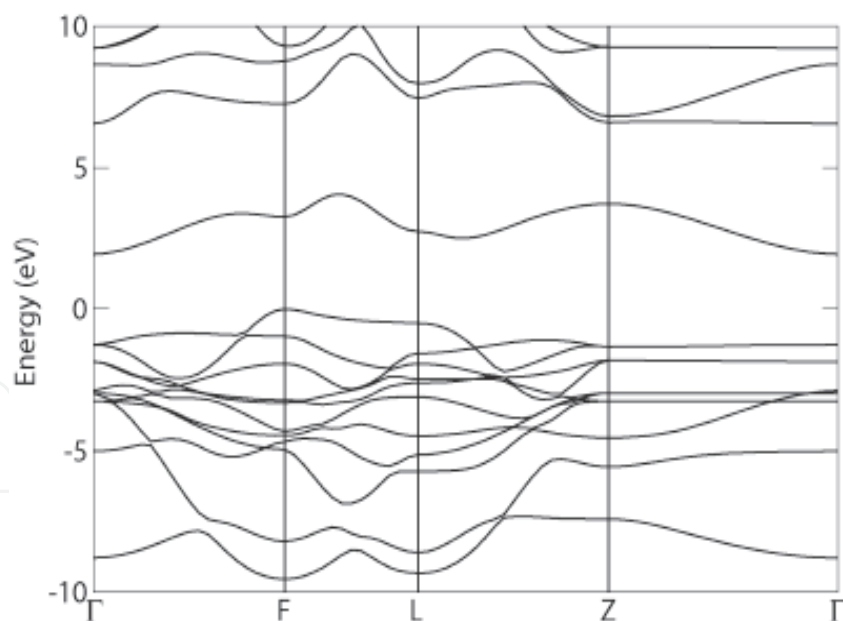


Fig. 2. GGA+U calculated bandstructure of CuBO_2 . The top of the valence band is set to 0 eV.

To gain a deeper understanding of the band structure features, we have plotted projections of the wave function for the VBM at F and the CBM at the Γ point through a (001) plane containing Cu, B, and O atoms, labeled (b) and (c) in Fig. 3. (David et al., 2009) A numerical breakdown of the states at the VBM shows that it contains $\sim 67\%$ Cu d character and $\sim 31\%$ oxygen p character, with B states effectively playing no role in the VBM makeup at F. This is

further evidenced by the charge density plot of the VBM (Fig. 3b) which clearly shows d-like orbitals on the Cu ions and p-like orbitals on the O ions, with the absence of any density on the B states.

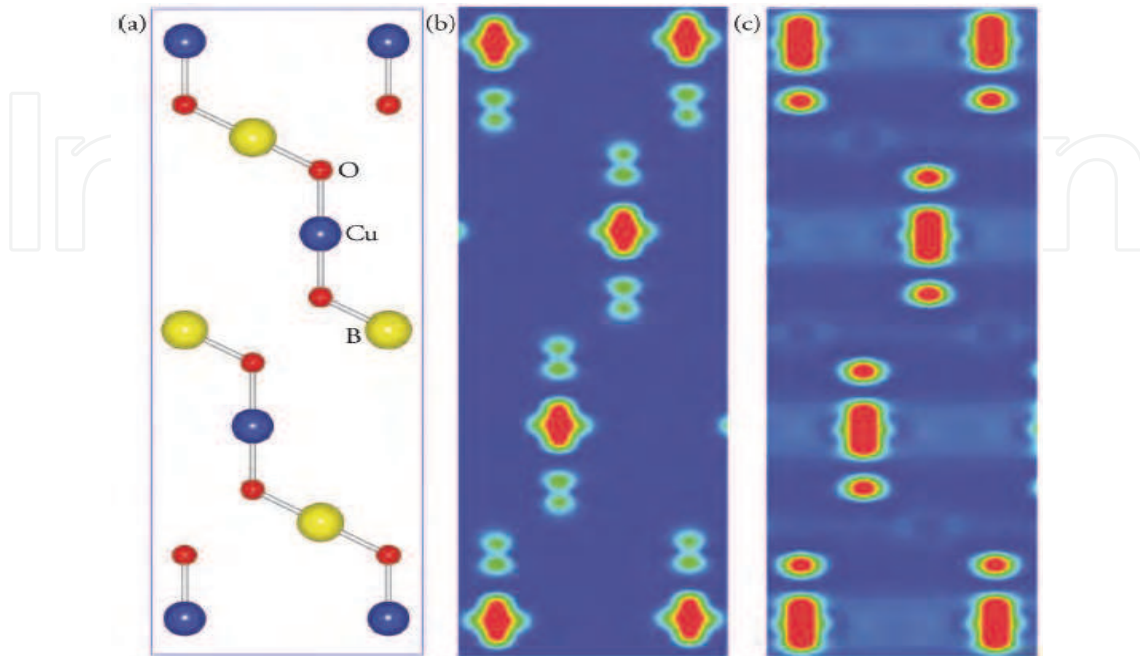


Fig. 3. Charge density contour plots showing the band edges of CuBO_2 through a (001) plane. (a) Structure of the cell in the (001) plane, (b) charge density of the VBM at F, and (c) charge density of the CBM at Γ , plotted from 0 eV (blue) to 0.003 eV (red) $\text{e} \cdot \text{\AA}^{-3}$.

2.1.2 CuAlO_2

Kawazoe et al. first reported synthesis of CuAlO_2 as a p-type TCO material based on the copper I oxides such as CuAlO_2 , CuGaO_2 , and SrCu_2O_2 with chemical modulation of valence band. (Kawazoe et al., 1997) In spite of several merits of CuAlO_2 as a p-type TCO, the main hurdle is its low electrical conductivity compared to the n-type TCO. Therefore, different methods such as high temperature solid-state reaction, hydrothermal method, ion exchanges, and sol-gel method etc. have been proposed to prepare CuAlO_2 . (Ghosh et al., 2009) Each copper atom of CuAlO_2 is linearly coordinated with two oxygen atoms to form an O-Cu-O dumbbell unit placed parallel to the c-axis. Oxygen atoms of the O-Cu-O dumbbell link all Cu layers with the AlO_2 layers. After the report of p-type semiconducting, transparent CuAlO_2 thin film, a research field in device technology has emerged, called 'transparent electronics'. For the synthesis of CuAlO_2 thin films, the groups of Hosono, Gong, and Chattopadhyay used pulsed laser deposition, plasma-enhanced metalorganic chemical vapor deposition (PE-MOCVD), and dc sputtering, respectively. (Sheng et al., 2006) The electronic structures of CuAlO_2 were experimentally probed by normal/inverse photoemission spectroscopy (PES/IPES). The Fermi energy determined experimentally was set to zero in the energy scale in the three spectra, as shown in Fig. 4.

A band gap was observed between the valence band edge in the PES spectrum and the conduction band edge in the IPES spectrum. The band gap estimated was about 3.5 eV. The Fermi energy lies around the top of the valence band. The origin of the energy axis is the Fermi level which was determined using Au deposited on sample. These results mean that

CuAlO_2 is a transparent p-type semiconducting material, which has excellent potential for use in optoelectronics device technology. Fig. 5 shows the emission current (I) versus macroscopic field (E) curve of CuAlO_2 thin films deposited on glass substrate as a function of the anode-sample separations (d). (Banerjee & Chattopadhyay, 2004)

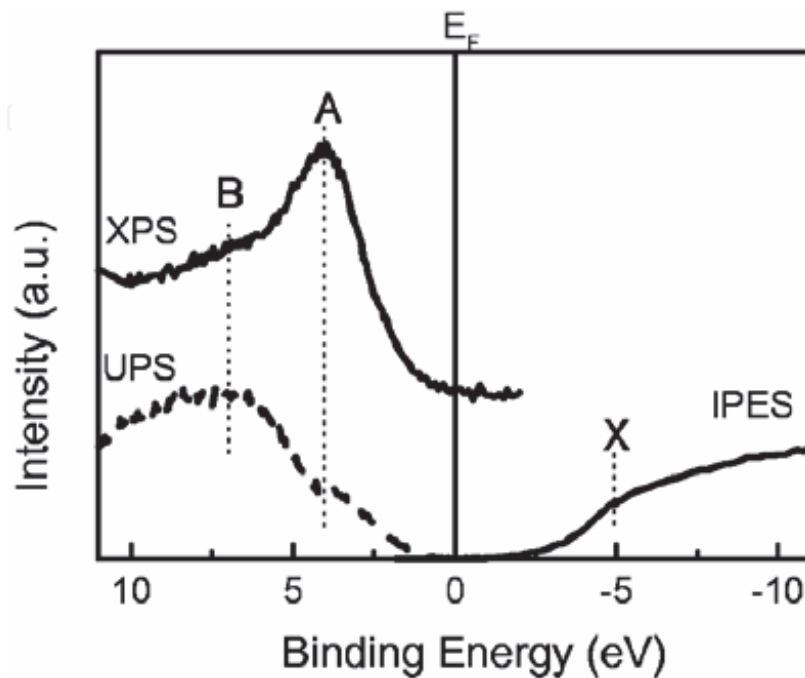


Fig. 4. Photoemission and inverse photoemission spectra of the valence and conduction region of CuAlO_2 .

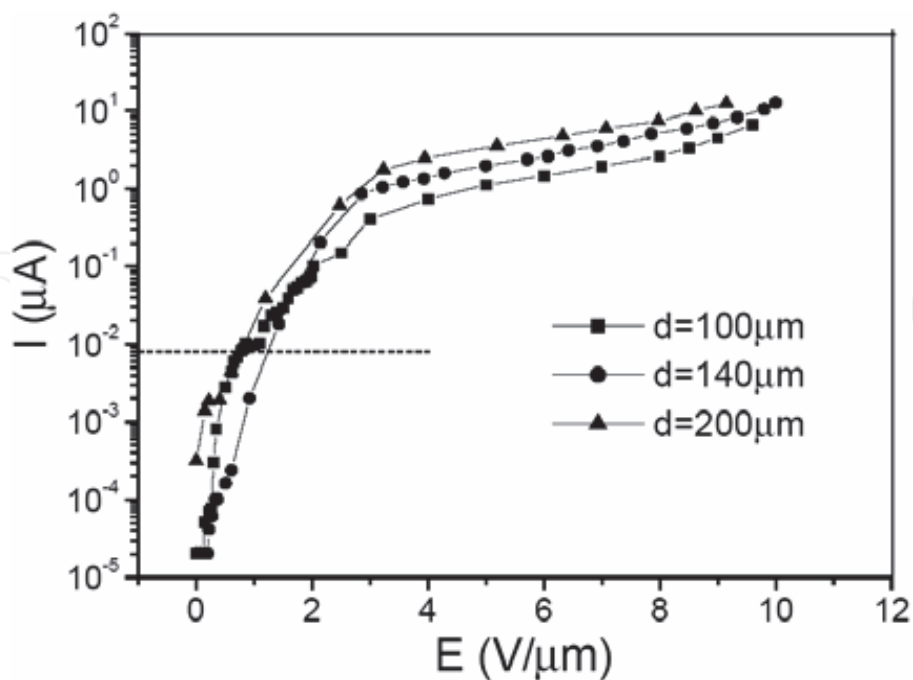


Fig. 5. Plot of emission current versus macroscopic field of CuAlO_2 thin film on glass substrate.

2.1.3 CuGaO₂

CuGaO₂ is a p-type TCO with E_g of ~ 3.6 eV. CuGaO₂ has a larger lattice constant of the a-axis, $a = 2.98$ Å, than CuAlO₂ ($a = 2.86$ Å). A polycrystalline thin film of CuGaO₂ prepared by rf sputtering method was obtained in an amorphous state by post-annealing for crystallization at 850 °C for 12 h under nitrogen atmosphere. And its activation energy was roughly estimated to be about 0.22 eV. The conductivity at room temperature was about 5.6×10^{-3} S·cm⁻¹. (Sheng et al., 2006) The electrical conductivity, carrier (positive hole) density, and Hall mobility of epitaxial CuGaO₂ films at room temperature were respectively 6.3×10^{-2} S·cm⁻¹, 1.7×10^{18} cm⁻³, and 0.23 cm²·V⁻¹·s⁻¹, which were prepared on a-Al₂O₃(001) single-crystal substrates by PLD without post-annealing treatment and it were superior to those of the polycrystalline thin films of CuGaO₂. The films were grown epitaxially on the substrates in an as-deposited state. The films have high optical transparency ($\sim 80\%$) in the visible region, and the energy gap of CuGaO₂ for direct allowed transition was estimated to be 3.6 eV. (Ueda et al., 2001)

2.1.4 CuInO₂

The CuInO₂ system, which is copper-based delafossites, has been particularly interested because it can be doped both p-type (with Ca) and n-type (with Sn), allowing p-n homojunctions to be produced by applying doping of an appropriate impurity and tuning the deposition conditions. (Yanagi et al., 2001a, 2002b) On the other hands, no similar trend like CuInO₂ has ever been observed in any other semiconductors because it has the largest reported band gap of 3.9 eV. The conductivity of CuInO₂ films reported by Yangagi et al. shows about $\sim 10^{-3}$ S cm⁻¹ when it was grown by PLD from phase-pure CuInO₂ targets. (Yanagi et al., 2001) It has been smaller than that of the other p-type TCOs. However, Teplin et al. used Cu₂In₂O₅ as a target to deposit single phase undoped and Ca-doped CuInO₂ thin films because the oxygen-rich Cu₂In₂O₅ phase of Cu-In-O is easily prepared by solid-state synthesis in air. (Teplin et al., 2004)

2.1.5 SrCu₂O₂

SrCu₂O₂ (SCO) is one of the few non-delafossite p-type oxides. In some groups, the properties of SCO deposited under working oxygen pressure of 5.25×10^{-3} mTorr and 300 °C are measured. Roy et al. reported the performance of SCO films with copper formate (Cu(CH₃COO)₂) and strontium acetate (Sr(CH₃COO)₂), which were chosen as starting precursors. (Roy et al., 2003) Stoichiometric amounts of Copper formate and Strontium acetate were prepared as separate aqueous solutions and mixed just before application (otherwise copper acetate precipitated) and were sprayed on quartz substrates at ~ 250 °C. Non-doped and K-doped p-type SCO thin films were first deposited by Kudo et al. (Kudo et al., 1998) And the PLD technique has been used to fabricate Ca-doped SCO thin films on quartz glass substrates. In case of the synthesis of SCO, a p-type transparent conducting oxide by a chemical solution route as well as the conventional PLD method, for SCO by the chemical solution route, samples were made by spraying deposition on quartz substrates using an aqueous solution of copper formate and strontium acetate. The X-ray diffraction (XRD) spectra of as-deposited thin-film samples for different substrate temperatures had only single (202) peak of SCO films. (Sheng et al., 2006) In this case, as increase the deposition temperature, the intensity of the (202) peak was increased. And also, the transmittance of SCO films is observed to depend on deposition temperature. On increasing the deposition temperature, the average transmission was decreased. The $(ah\nu)^2$

versus $h\nu$ plot is shown, from which the direct allowed band gap can be estimated; it was found to be about 3.2 eV for films deposited at 350 °C. The conductivity of the film deposited in room temperature was obtained as $8.2 \times 10^{-2} \text{ S cm}^{-1}$, which is decreased as $5.4 \times 10^{-2} \text{ S cm}^{-1}$ deposited at 400 °C. (Roy et al., 2003)

2.2 n-type TCO

While the development of new TCO materials is mostly dictated by the requirements of specific applications, low resistivity and low optical absorption are always significant prerequisites. There are basically two strategies in managing the task of developing advanced TCOs that could satisfy the requirements. The main strategy dopes known binary TCOs with other elements, which can increase the density of conducting electrons. More than 20 different doped binary TCOs were produced and characterized by n-type TCOs, of which ITO was preferred, while Al-doped ZnO (AZO) and Ga or Ga₂O₃-doped ZnO (GZO) come close to it in their electrical and optical performance. The TCOs have been intensively studied for their potential in optoelectronic applications, including for the manufacture of OLEDs. It has been well known that ITO is the most popular TCO, because of its high conductivity and transparency. (Kim et al., 1996) However, its chemical instability, toxic nature and high cost, combined with the diffusion of indium into surrounding organic materials, have stimulated efforts to find an alternative. (Kim et al., 2000)

Among these materials, one of most promising candidates is AZO which has sufficiently high conductivity and a transmittance of over 90% in the visible range, even in samples grown at room temperature. (Chem et al., 2000) Recently, it has been reported that optimized AZO films could replace ITO as an anode material in OLED applications. In comparison with ITO, AZO films are more stable in reducing ambient circumstance, more readily available, and less expensive. Because of these characteristics, AZO is often used as an anode material in photoelectronic devices such as solar cells, flat panel displays and OLEDs. (Yang et al., 1998; Ott & Chang, 1999; Wang et al., 2006; Deng et al., 1999) Previously, we reported that the AZO can be successfully adopted as a TCO on a flexible polymer polyethersulphone (PES) substrate for flexible OLED application. (Park et al., 2007) Because the anode materials in an OLED are in contact with organic molecules, both their surface chemical properties and their morphology affect the adhesion and alignment of molecules on the surface. (Guo et al., 2005)

Therefore, a microscopic understanding of wettability in solid surfaces is fundamentally interesting and practically valuable. Furthermore, the absorption of water on metal-oxide surfaces is an important subject in its own right, due to its crucial role in gas sensors, catalysis, photochemistry and electrochemistry. It is well known that the measurement of water contact angle (WCA) could reveal much useful information about characteristics of surface nanostructure and morphology. (Soeno et al., 2004) However, there have been few studies of the surface wettability of the transparent conducting oxide AZO thin film. AZO films with resistivity of $\sim 8.5 \cdot 10^{-5} \text{ W} \cdot \text{cm}$ was reported by Agura et al. (Agura et al., 2003) An even lower resistivity was reported for GZO, $\sim 8.1 \times 10^{-5} \text{ W} \cdot \text{cm}$. (Park et al. 2006) This r is very close to the lowest resistivity of ITO of $7.7 \times 10^{-5} \text{ W} \cdot \text{cm}$, with a free carrier density of $2.5 \times 10^{21} \text{ cm}^{-3}$. (Ohta et al., 2000) The phase-segregated two-binary systems include ZnO-SnO₂, CdO-SnO₂, and ZnO-In₂O₃. In spite of the expectations, the electrical and optical properties of the two-binary TCOs were much inferior to those of ITO. Accordingly, the ternary TCO compounds could be formed by combining ZnO, CdO, SnO₂, InO_{1.5} and GaO_{1.5} to obtain Zn₂SnO₄, ZnSnO₃, CdSnO₄, ZnGa₂O₄, GaInO₃, Zn₂In₂O₅, Zn₃In₂O₆, and Zn₄In₂O₇.

However, since Cd and its compounds are highly toxic, the utilization of these TCOs is limited, though they have adequate electrical and optical properties. Other binary TCOs were synthesized from known binary TCOs and also from non-TCO compounds, such as $\text{In}_6\text{WO}_{12}$ and the p-type CuAlO_2 . All of the TCOs discussed above are n-type TCOs. In addition, p-type doped TCOs were also developed and could find interesting future applications, in particular as a new optoelectronic field like "transparent electronics". (Banerjee & Chattopadhyay, 2005)

The need to produce n-type TCOs with higher conductivity and better transmission, without relying on In, gave rise to research and development effort for new TCOs. Recently, mobility with more than twice that of commercial ITO was achieved in Mo-doped In_2O_3 (IMO), and this material showed that the conductivity can be significantly increased with no changes in the optical transmittance upon doping of Mo. (Meng et al., 2001; Yoshida et al., 2004) Electronic band structure of IMO was investigated by Medvedeva, it was revealed that the magnetic interactions which had never been considered to play a role in combining optical transparency with electrical conductivity ensure both high carrier mobility and high optical transmittance in the visible range. (Medvedeva, 2006)

Recently, new thin film geometries were also explored by Dingle *et al.* in search of TCO films with higher conductivity. (Dingle et al., 1978) They showed that higher conductivity could be obtained by doping modulation, which spatially separates the conduction electrons and their parent impurity atoms (ions) and thereby reduced the effect of ionized and impurity scattering on the electron motion. Rauf used a zone confining process to deposit ITO with $r = 4.4 \times 10^{-5} \text{ W} \cdot \text{cm}$ and $m = 10^3 \text{ cm}^2/\text{Vs}$. (Rauf, 1993) The highly and lowly doped regions were laterally arranged in the films, rather than vertically as in superlattice structures. A theoretical outline of a method to engineer high mobility TCOs was presented by Robbins and Wolden, based on the high mobility transistor structure discovered accidentally by Tuttle *et al.* (Robin & Wolden, 2003) The film should consist of alternating thin layers of two semiconductors. One layer provides a high density of carriers, while the second is a high mobility material. Electrons are supplied by the former and transported in the latter, mitigating the limitations of ionized impurity scattering. (Tuttle et al., 1989) The model of Robbins and Wolden assumes that the electrons move into the high mobility material in response to differences in electron affinity. However, the success of the proposed TCO design depends upon controlling the layer thickness at nano dimensions, (e.g. $\sim 5 \text{ nm}$). In addition, this approach depends on having materials of excellent quality and compatible crystal structure in order to avoid problems related to interface defects. TCO materials with magnetic properties, which are ferromagnetic semiconductors with a Curie temperature well above room temperature, have also been explored recently, as they could be used for second generation spin electronics and as transparent ferromagnets. Ueda *et al.* reported that Co doped ZnO thin film ($\text{Zn}_{1-x}\text{Co}_x\text{O}$) with $x = 0.05 - 0.25$, had a large magnetic moment of 1.8mB per Co ion for $x = 0.05$. High-temperature ferromagnetism was subsequently found by other groups, with varying magnetic moments. (Ueda et al., 2001)

2.3 Indium-based TCOs

In fabricating OLED devices, ITO film among the transparent conductive oxide (TCO) films is widely used as an anode layer, because of its high transparency in the visible light range, low conductivity, and high work function ($\sim 4.8 \text{ eV}$). In majority of cases, a thin layer of a mixed ITO made of 9~10 mol % of tin oxide in indium oxide on a transparent substrate is used. However, conducting oxides such as pure tin oxide, Ga-In-Sn-O (GITO, 5.4 eV), Zn-In-Sn-O

(ZITO, 6.1 eV), Ga-In-O (GIO, 5.2 eV), and Zn-In-O (ZIO, 5.2 eV) films composed with In, Sn, Ga, Zn, and O components have particularly interesting transparency and conducting properties. They possess better characteristics than ITO such as a larger work function. Conducting polymer, TiN, and semitransparent at thicknesses that are suitable due to high conductivity as an electrodes. Besides, the FOLEDS has led to the utilization of the ITO or the organic conductors, such as; polyaniline(PANI) deposited on various plastic substrates of polyethylene terephthalate(PET), polyethylene naphthalate(PEN), polyimide(PI), polycarbonate(PC), polypropylene adipate, and acrylic polymer. The following paragraphs explain in detail the solutions found in the literature for realizing the anode. Among the many factors determining the performance of OLED devices, the interface between the organic hole transport layer (HTL) and the anode layer plays an important role in controlling the efficiency of the charge carrier injection into the emitting layer.(Li et al., 2005; Chan & Hong, 2004) The insertion of various thin insulating films, such as WO_3 , NiO, SiO_2 , ZrO_2 , Ta_2O_5 , and TiO_2 , between the ITO anode and the HTL layer, was found to improve the performance of the OLEDs, which was explained by the energy level alignment or tunneling effect.(Qiu et al., 2003; Huang, 2003; Mitsui & Masumo, 2003; Lu & Yokoyama, 2003; Ishii et al., 1999; VanSlyke et al., 1996) In addition, the modification of the work function of the ITO surface was reported by doping it with Hf atoms using a co-sputtering technique or inserting a conducting oxide layer, i.e., IrO_x , which increases the work function of the ITO surface through dipole formation.(Chen et al., 2004; Kim & Lee, 2005)

Although many thin-film deposition techniques, such as sputtering or chemical vapor deposition, have been used to obtain an ultra-thin interfacial layer between the HTL and anode, these methods are not suitable for obtaining a high quality ultra-thin interfacial layer with a sub-nm range thickness. Recently, atomic layer chemical vapor deposition (ALCVD) has been widely used in many application areas which require precise thickness controllability and low structural defects, because the ALCVD process is based on surface adsorption- and saturation-controlled deposition kinetics. This results shows the effects of ALCVD treatment performed both at room temperature (RT) and at various temperatures up to the typical HfO_2 deposition temperature (300 °C) using tetrakis(ethylmethylamino) hafnium (TEMAH; $\text{Hf}[\text{N}(\text{CH}_3)\text{C}_2\text{H}_5]_4$) as the precursor on OLEDs. The binding and molecular structures of the HfO_x layer formed on the ITO surface were analyzed by X-ray photoelectron spectroscopy (XPS) and near-edge X-ray absorption fine structure (NEXAFS) spectroscopy.

Compared to the control sample without any treatment, the sample treated for 5 cycles at RT, which was referred to as RT-5C, exhibited significantly improved OLED performance, i.e., a decrease in turn-on voltage as depicted in the inset of Fig. 6(a) and an increase in brightness.

Because of the high current flow and subsequent increase in brightness mainly originating from the increased hole injection efficiency from the ITO anode into the organic layer, we found that the 5 cycle treatment at RT by the ALCVD process is an effective method of improving hole injection efficiency.(Shrotriya & Yang, 2005) However, when the number of ALCVD cycles was increased at RT, the turn-on voltage increased and the brightness decreased as compared to the control sample as shown in Fig. 6. This is believed to be caused by the formation of an insulating layer and the consequent retardation of the hole injection. With the increase of the deposition temperature, the electrical and optical characteristics of the OLEDs showed similar or worse performance when compared to the control sample as a function of deposition cycles as shown in Figs. 7 and 8.

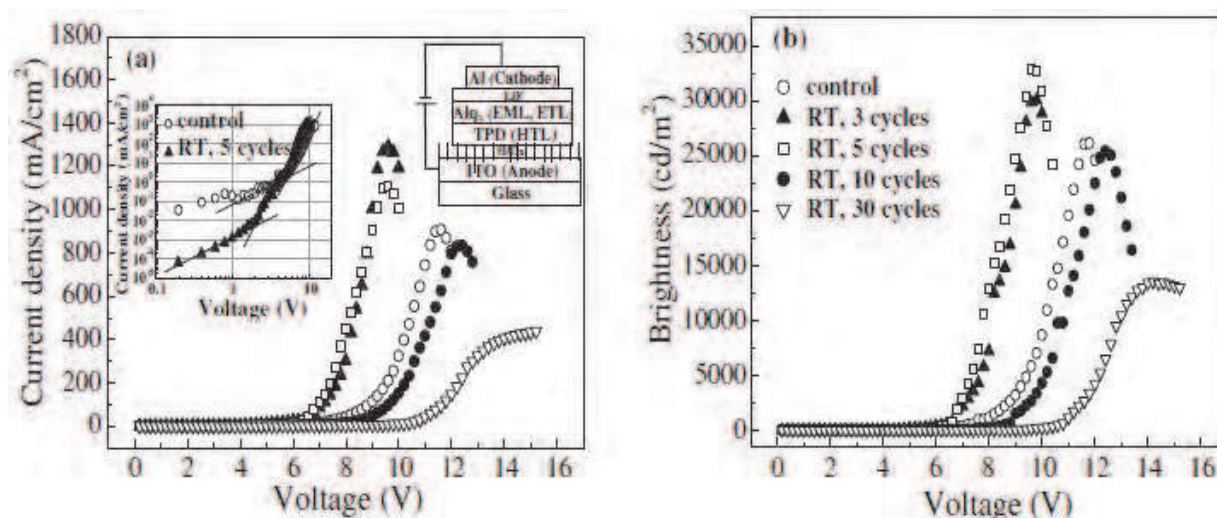


Fig. 6. (a) J-V, (b) B-V characteristics of OLEDs treated without and with ALCVD-HfO_x at room temperature as a function of deposition cycles.

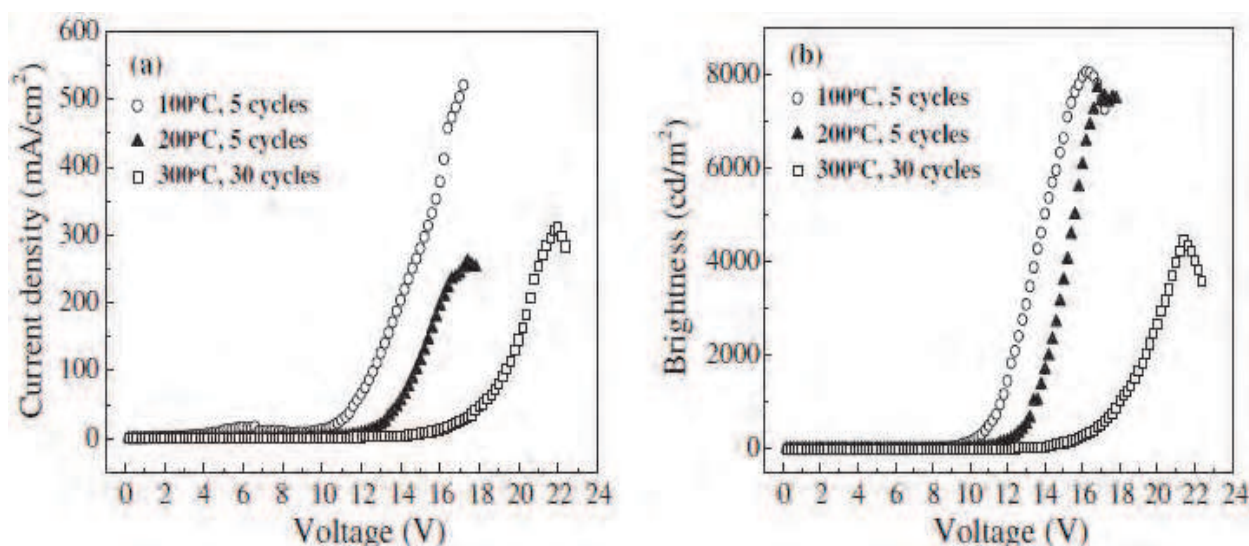


Fig. 7. (a) J-V, (b) B-V, and (c) power efficiency characteristics of OLEDs treated with ALCVD-HfO_x at 100, 200, and 300 °C as a function of deposition cycles.

The Hf precursor formed Hf-O bonding having a high dipole moment with the underlying ITO network, and the subsequent bias-induced realignment of the anode Fermi level and highest occupied molecular orbital (HOMO) of the HTL lowered the band offset with the top HTL by modifying the work function of the ITO surface, as shown in Fig. 9.

However, the existence of the ultra-thin HfO_x layer did not retard the hole injection from the anode due to the tunneling effect. When the number of cycles or deposition temperature was increased, the peaks caused by the unoccupied hybridized orbitals of Hf and O appeared in the lower photon energy range, which confirmed the formation of an electrically insulating HfO_x layer. The O K edge NEXAFS spectra of the 300 °C-30 cycles sample were directly related to the oxygen p-projected density of states of ITO overlapped with that of HfO₂, which consists of the four unoccupied hybridized orbitals, Hf 5d+O 2p_π, Hf 5d+O 2p_σ, Hf 6s+O 2p, and Hf 6p+O 2p of the HfO₂ film. (Cho et al., 2004) The formation

of a physically thick insulating HfO_x layer between the anode and HTL, as confirmed by the NEXAFS measurement, significantly deteriorated the OLED performance, as previously shown in Figs. 6 and 7.

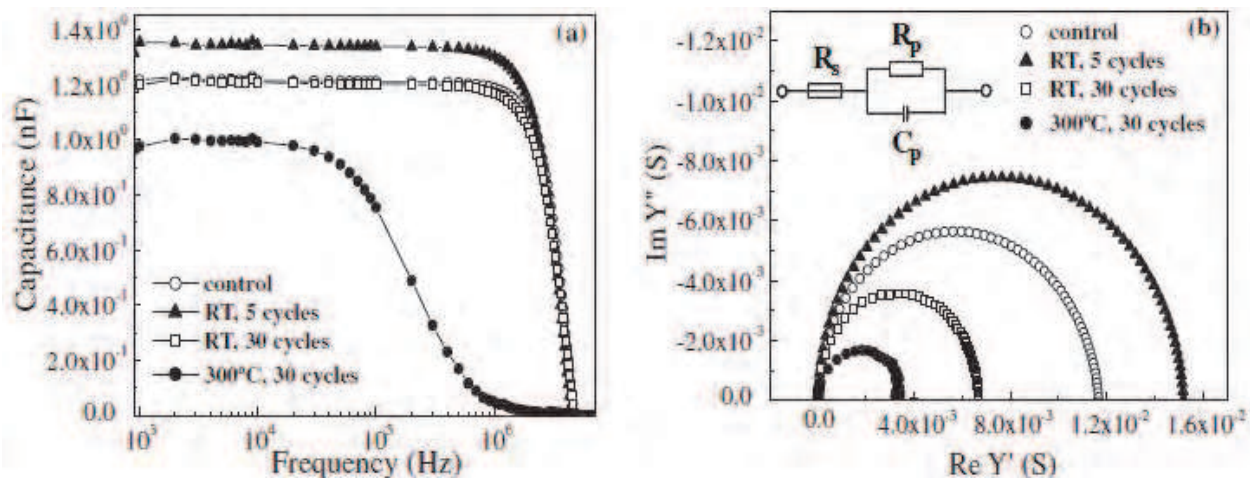


Fig. 8. (a) C-f characteristics and (b) Cole-Cole plots of OLEDs without and with surface treatment.

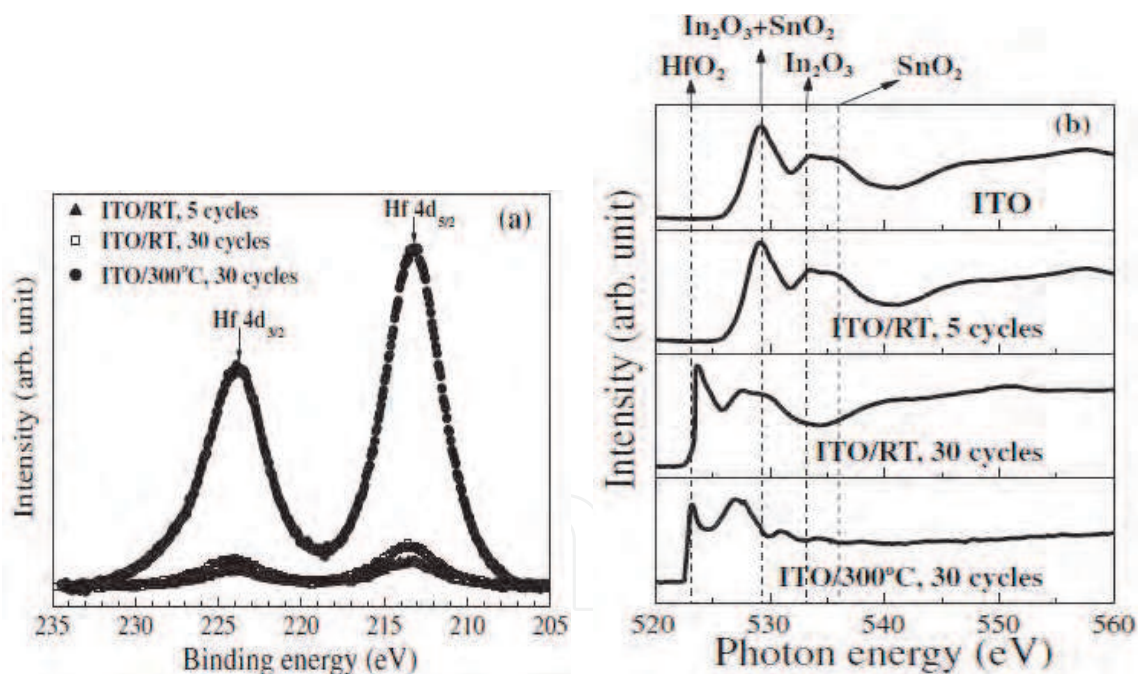


Fig. 9. (a) Hf 4d peak in the XPS peak spectra and (b) NEXAFS spectra of the O K edge features of the ITO surface as a function of TEMAH deposition conditions.

In order to measure the relative work function for a pristine ITO anode and ITO anodes modified by the different surface treatments of HfC_x , HfO_x and HfO_2 for 5 cycles, we carried out Kelvin probe current measurements as a function of the substrate bias by using the Kelvin probe microscopy (KPM) system in UHV conditions, as shown in Fig. 10. (Sohn, 2008) The applied bias (V_{App}) of the surface potential difference between the Kelvin probe tip and the pristine ITO substrate (V_{ITO}) under different HfC_x , HfO_x and HfO_2 treatment conditions

were, respectively, shifted to -0.2, 0.4, -0.9 V, which resulted in improved or deteriorated device properties. The increased work function of the HfO_x -treated ITO anode reduced the barrier height for hole carrier injection in OLEDs compared to that of the HfC_x treatment without an oxidant or the HfO_2 treatment with a high deposition temperature.

And also, Sugiyama et al. suggested the three factors such as C-containing contaminants, the O/In ratio, and the In/Sn ratio for the increase of the ITO work function. In order to be utilized as excellent anode in OLEDs, however, the ITO film has to solve some problems such as formation of a defect region by diffusion of oxygen or In metal into the organic material layer, low transparency in the blue light range, and discord of the energy level alignment by difference between the ITO work function and HOMO level of a typical HTL. In order to increase the work function of ITO, a number of investigations were reported, such as the surface treatments under O_2 , N_2 , H_2 , and $\text{N}_2\text{-H}_2$ condition, or the insertion of an anode interfacial layer with insulating wide band gap between the HTL and the anode.

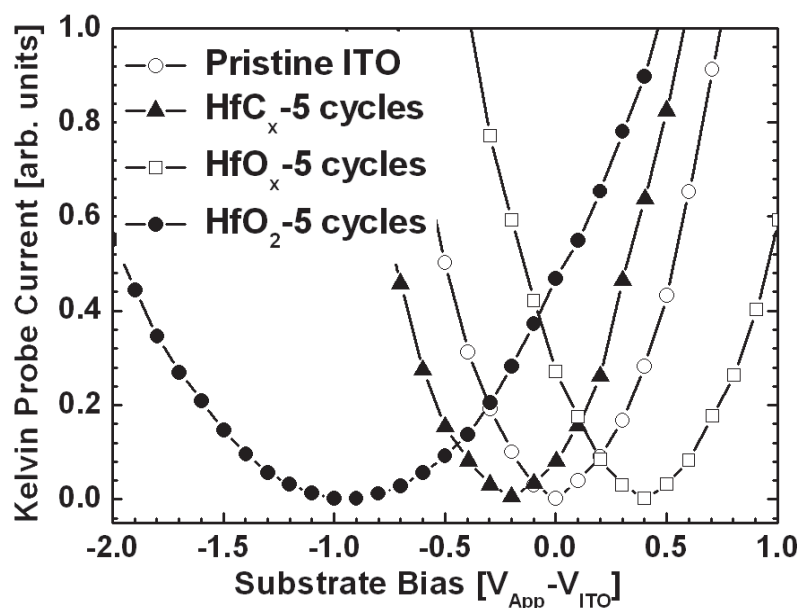


Fig. 10. Kelvin probe current for a pristine ITO anode and an ITO anode modified by HfC_x , HfO_x and HfO_2 surface treatment for five cycles as a function of substrate bias. The applied bias (V_{App}) has been shifted by the surface potential difference between the Kelvin probes tip and the pristine ITO substrate (V_{ITO}).

The development of the TCO films such as Ga-In-Sn-O (GITO, 5.4 eV), Zn-In-Sn-O (ZITO, 6.1 eV), Ga-In-O (GIO, 5.2 eV), and Zn-In-O (ZIO, 5.2 eV) TCO films composed with In, Sn, Ga, Zn, and O materials. Especially, the oxygen plasma or UV ozone treatments on ITO surface can increase the work function of ITO and remove the carbon contamination of ITO surface. However, the improvement by oxygen plasma, widely used in OLEDs, is strongly dependent on processing conditions. Recently, Hung *et al.* reported that the polymerized fluorocarbon film formed on ITO surface can improve the charge carrier injection because it has a high ionization potential and relatively low resistance. The OLEDs with fluorocarbon/oxygen mixture showed the improved device performance with enhancing the holes injection by remove the carbon contamination on ITO surface and also accelerate the fluorine bonding directly to indium or tin on the ITO surface.

In order to determine the effect of the CF_x treatment, the conductance, capacitance, and impedance were respectively measured for the devices with and without the CF_x treatment in the frequency range of 10 Hz to 10 MHz for a zero bias voltage. In the low frequency region, the CF_x treated ITO anode had a higher capacitance than the device with the untreated ITO anode, which is related to the enhancement of carrier injection and space charge formed by the injected carriers. (Kim et al., 2008)

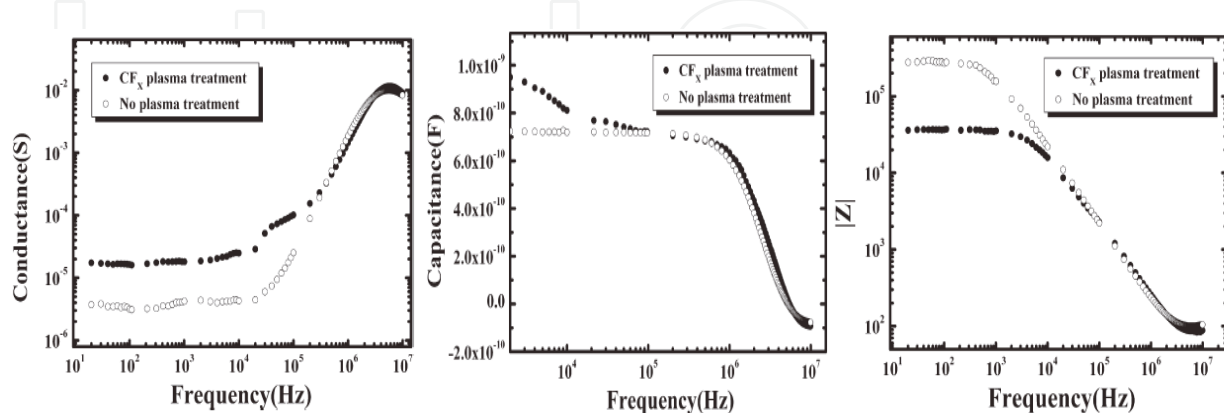


Fig. 11. Variation in conductance, capacitance, and impedance as a function of frequency in the device with and without the CF_x plasma treatment.

2.4 Zinc-based TCOs without indium

The ITO is mostly used as a promising candidate material for TCO films due to many advantages, such as high conductivity ($\sim 10^{-4} \Omega \text{ cm}$), high transmittance ($\sim 85\%$) in visible light range, high uniformity, and high work-function ($\sim 4.8 \text{ eV}$). (Minami, 1999; Miyata, 1997; Shan, 2003; Yan, 1998) However, it was found that they have often been limited in their application because of the frequent necessity to optimize electrical, optical, and chemical properties for specialized applications. For example, the conventional ITO films have some substantial problem such relatively high deposition process ($>300 \text{ }^\circ\text{C}$) to get a low resistivity, drop of optical transmittance under H_2 plasma condition, and rising price due to indium exhaustion within a few years. (Han, 2001; Hirata, 1996; Honda, 1995; Minami, 1984; Park, 2006a, 2006b) The amorphous ITO film deposited at a low temperature has a low resistance to moist heat, which leads to a degradation in its conductivity and the light transmittance with time. Moreover, the chemical and electronic properties of ITO are far from optimum for current and future generation OLEDs. Drawbacks include deleterious diffusion of oxygen and In into proximate organic charge transporting/emissive layer, imperfect work function alignment with respect to typical HTL, HOMO level, and poor transparency in the blue region. For the purpose of improving TCO film properties, new materials consisting of ternary compound oxides based on ZnO were investigated. For example, In-doped ZnO (IZO), Al-doped ZnO (AZO), Ti-doped ZnO (TZO), and Si-doped ZnO (SZO) have been attracted, which are considerable attention as an alternative materials for ITO. Recently, zinc oxide or impurity (B, Al, Ga, In, and Zr) doped zinc oxide films have been investigated as alternate materials to ITO for OLEDs because zinc oxide is nontoxic, inexpensive and abundant. It is also chemically stable under exposure to hydrogen plasma that is commonly used for the fabrication of thin film transistor-liquid crystal display (TFT-LCD). Kim et al., investigated the Zr-doped ZnO (ZZO) thin film grown by PLD on glass substrates as a

function of oxygen deposition pressure and film growth temperature for OLEDs.(Kim et al., 2003) For a 200-nm-thick ZZO film grown at 250°C in 1 mTorr, a resistivity of $5.6 \times 10^{-4} \Omega \cdot \text{cm}$ and optical transmittance of 84% were measured. These results demonstrate that ZZO is a good anode material because the OLEDs fabricated on ZZO anodes exhibit external EL quantum efficiency comparable to a control device fabricated on commercial ITO.

Further increase of the good performance at ZnO based TCO films can be achieved through improving crystallinity by preparing single crystal or hetero-epitaxial ZnO films and/or increasing grain size in film by the post-annealing method. And the improvement of the electron mobility can be obtained by new composition materials by the addition of impurity dopants, such as Al, Ga, In, Ti and so on. Recently, TiO_2 has become the subject of many investigations for applications in optical coatings because of their good properties such as a high refractive index, high transparency, excellent water resistance, and thermal stability. However, since the conventional RF-magnetron sputter (RFS) system for TCO film deposition has consist with a system of the target and the substrate facing with each other, the particles with high energy such as γ -electrons, neutral Ar particles, and negative oxygen ions collide with the substrate. In this study, facing target sputtering (FTS) apparatus was designed to enhance the preciseness of manufactured thin film and the sputter yield rate with depositing film by forming higher density plasma in the electrical discharge space.(Kim, 2001; Noda, 1999, Nose, 1999) TiO_2 -doped ZnO films, in comparison with the ZnO films doped with Group III elements, have more than one charge valence state. In this study, the electrical and optical properties of TiO_2 -doped zinc oxide (TZO) films with various deposition thicknesses by FTS system were compared to those of the films made by conventional RFS method. For more details, the relations in the resistivity, carrier concentration and mobility, film density, and intrinsic stress in the films as a function of the deposition method with the FTS and conventional RFS system were analyzed.

The TZO films were deposited on slide glass substrates at RT by FTS and RFS methods, respectively. Target materials were made up of TiO_2 and ZnO powders with purity of 99.999 % that were calcined at 1000 °C in Ar atmosphere for 2 hours. The mixture with composition ratios was prepared for the target the composition ratios were selected as $\text{TiO}_2 : \text{ZnO} = 2 : 98$ weight percent (wt.%), and we will refer to the films deposited with the target as the TZO film. For FTS system, two circular targets with a size of 3 inch are located horizontally facing with each other, and more detail FTS structure was explained at previous report.(Kim, 2009) The applied RF-powers were respectively 120 W and 80 W for the film deposition using FTS and RFS system, the working pressure was set at 2×10^{-3} torr, and a pure Ar gas was used as discharge gas. Two circular targets with a size of 3 inch are located horizontally facing with each other, and Nd alloy permanent magnets of 4700 Gauss for plasma confining magnetic field was mounted to the back of the target, which was adjusted by variation of the distance between both two targets. In order to control the heat of the system caused by the ion bombardment of the cathode, cooling water was supplied. We investigated the process characteristics of the FTS apparatus under various deposition thicknesses compared with the film by RFS system. FTS system is a high-speed and low deposition temperature method, which arrays two sheets of targets facing each other. Inserts plasma is arresting magnetic field to the parallel direction of the center axis of both targets, discharged from targets and accelerated at the cathode falling area. Thus, this system is a plasma-free sputter method in which substrate is located at far from plasma. And also, the temperature on substrate during film deposition was much lower than that of the conventional sputtering method. And also,

the prepared films using FTS system as a function of the distance from center to edge has the uniform thickness. An ultra violet visible spectrophotometer (UV-VIS, Shimadzu Co.) was used to analyze the optical properties of the film such as transmittance and optical energy bandgap (E_{opt}). Crystallographic properties of the TZO films were analyzed by X-ray diffraction (XRD, Rikagu Co.) patterns by using the $Cu-K\alpha$ ($\lambda = 1.54\text{\AA}$) line. Surface morphology of the film was observed by a scanning electron microscopy (SEM, Hitachi Ltd.) and an atomic force microscope (AFM, Veeco Instruments Inc.), and the film thickness was measured by a -step. Electrical resistances and hall mobility of the films were measured by the Hall effect measurement system (HEM-2000, EGK Co.) using Van der paw method.

Fig. 12 shows the optical transmittance spectra of various TZO films prepared by respectively FTS and RFS system as a function of the film thickness. Under the same film thickness, the oscillation peaks by maximum and minimum points using a distributed Bragg reflector show a similar tendency. TZO thin films prepared by conventional sputtering and FTS method showed similar optical transmittance over 80 % in visible light range with baseline of glass substrate, which can applied in various optoelectronics like next generation FPDs, touch panel, and so on. The absorption edges of TZO films deposited by FTS method have been blue shifted compared with the film prepared by RFS method at same film thickness. It means that the optical band gaps were increased as shown in the inset of Fig. 12, which is attributed to Burstein-Mott effect due to the increase of carrier concentration by film density. In insertion of Fig. 12, the optical band gap E_{opt} of the TCO films were calculated by the Tauc's relation (Chowdhury, 2000; Tauc, 1974)

$$(ah\nu) = B(h\nu - E_{opt})^n \quad (2)$$

, where a is the absorption coefficient, $h\nu$ is the energy of absorbed light, n is the parameter connected with distribution of the density of states and B is the proportionality factor.

The TZO films by FTS system with various deposition thicknesses show the higher E_{opt} values than that of the films by RFS system, which is well correspond to the improvement of resistivity due to increase of carrier concentration of the films in Fig. 13. The ΔE_{opt} as the increase of optical bandgap by Burnstine Moss effect was as below:

$$\Delta E_{opt} = (\hbar^2/2m^*) \cdot (3\pi^2)^{2/3} \cdot N^{2/3} \quad (3)$$

, where \hbar is Planck constant and m^* is effective mass.

Thus, the carrier concentration (N) is also increased when the optical bandgap is increased. The E_{opt} was increased from 3.4 to 3.5 eV at 100 nm film thickness when the TZO film was deposited by FTS system compared to those of the film prepared by the RFS system. The widening of the energy band gap with the TZO film could be due to the increase in the carrier concentration.

Fig. 13 shows the resistivity (left) and the carrier mobility (right) of the TZO films deposited by FTS and RFS system using Hall effect measurement. Usually, the resistivity (ρ) of film is in inverse proportion to film thickness, and relational expression is given by the equation:

$$\rho = R_s / t \quad (4)$$

, where R_s is the sheet resistance and t is the film thickness.

As shown in Fig. 13, the resistivity of TZO films is related to the carrier concentration and the Hall mobility. This indicates that the electrical conductivity of TZO films is due to the contribution from Ti^{4+} ions in the substitution sites of Zn^{2+} ions, interstitial atoms, and

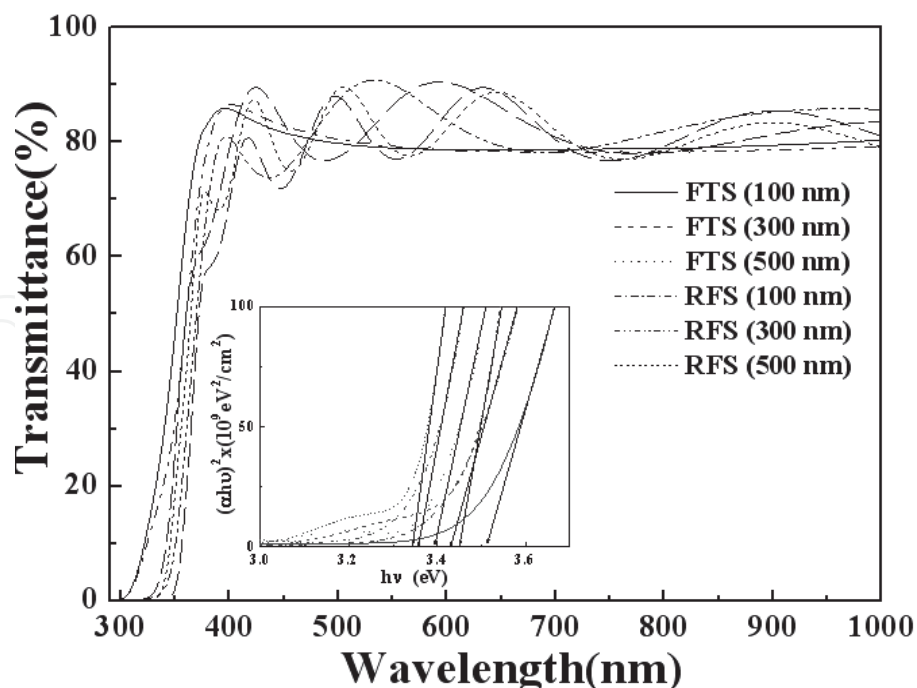


Fig. 12. Optical transmittance of TZO thin films deposited with deposition thickness of 500 nm on PEN substrate under various rf-power. The inset shows a plot of $ah\nu$ vs. $h\nu$ calculated from the optical transmittance spectra.

oxygen vacancies.(Chung, 2008) Finally, because the TCO film having both maximum conductivity and carrier mobility has a film density close to its theoretical density, it means that the electrical characteristics of the TCO films discussed here depend strongly on the grain size. More detail explanations will be discussed in Fig. 14 and 15.

However, the mean free paths were smaller than the grain size when the TCO films with the density showed lower than theoretical (not shown here). It is known that electron scattering at pores and voids within the grain is the major obstacle for electron conduction in the TZO films having a lower density. We thought that the scattering of the conduction electrons at the grain boundary during film deposition may be the major factor in determining the carrier mobility in TZO films. The electrical resistivity of TZO film deposited by FTS system showed about $5.0 \times 10^{-4} \Omega \text{ cm}$, which was lower than that of the film made by conventional sputtering method with about $7.5 \times 10^{-4} \Omega \text{ cm}$ at 500 nm film thickness. We thought that the enhanced property of the film by FTS method was caused by the influence of the film density and/or the mean free path because the FTS used in this study is a high speed and low temperature sputter method that promotes ionization of sputter gas by screw-moving high-speed γ -electrons which array two sheets of targets facing each other. The generated plasma was arrested magnetic field to the parallel direction of the center axis of both targets, discharged from targets and accelerated at the cathode falling area. Therefore, the application parts of the FTS system will be extend because the FTS is a plasma-free sputter method in which the substrate is located apart from plasma.

Fig. 14 shows the XRD spectra of TZO films deposited by the FTS and the RFS with various film thicknesses. As increasing deposition thickness, the RF-sputtered films show the hexagonal wurtzite structure and has strong ZnO(002) peak of preferred orientation, together with relatively weak ZnO(103) peak.(Choi, 2005) It is notable that the intensity of ZnO(002) peak for the TZO films by the RFS system slightly increased with increasing

deposition thickness. On the other hand, the intensity of the TZO films by the FTS system shows the weak (103) peak. It could be attributed to Ti atoms in TZO films. In Fig. 13, the resistivity of TZO films by both FTS and RFS system are significantly decreased while the deposition thicknesses are increase from 100 nm to 300 nm, however, and the value was almost saturated at 500 nm thickness. For the TZO film with optimum properties, we suggest that the crystallinity between (002) and (103) peaks was almost same in case of the film with 300 nm thickness as shown in Fig. 14(a). For more detail, the grain sizes of the films are calculated using Scherrer formula from XRD spectra as below:(Mardare, 2000)

$$D=(0.9\lambda)/(B\cos\theta) \quad (5)$$

where D is grain size, X-ray wavelength(λ) is using the Cu-K α line(1.5405 Å), B is the full width at half maximum (FWHM) of (002) and (103) peaks, and θ is diffraction angle.

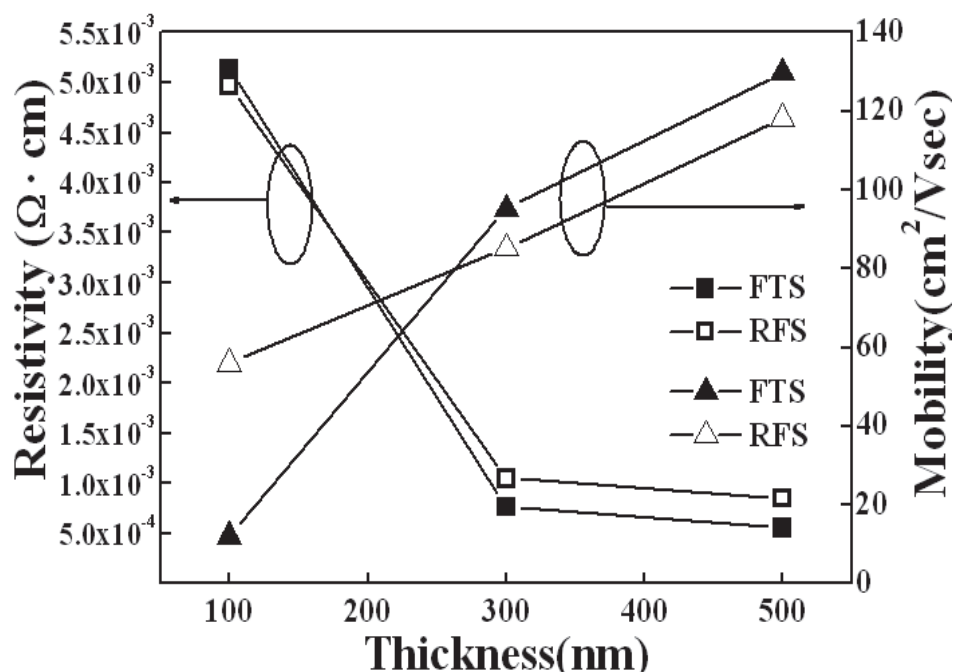


Fig. 13. Resistivity (left) and carrier mobility (right) of the TZO thin films as a function of the film thickness on glass substrate.

From the formula (4), the measured grain sized was varied from 105 nm to 155 nm. Thus, we thought that the film density was also improved as increase of the crystallinity as a function of the film thickness. The enhancement of the crystallinity and density in the TZO film can influenced on the conductivity of the film. The mean free path of the carrier as increase of the film density was also increased, which was resulted in increase hall mobility, as shown in Fig. 13.(Li et al., 2009)

Fig. 15 shows the SEM images of the TZO films with various deposition thickness using the FTS (a-c) and RFS (d-f) system. As increase film thickness, the grain sizes at both systems were proportionally increased. The film density was significantly improved while the deposition thicknesses are increase from 100 nm to 300 nm. However it was deteriorated at 500 nm thickness at both systems. The results are well agreed with the electrical properties in Fig. 13. The grain shapes of the TZO films by FTS system looks like the horizontal growth of (103) plane in Fig. 15(a)-(c). And also, the TZO films by RFS system in Fig. 15(d)-(f) looks

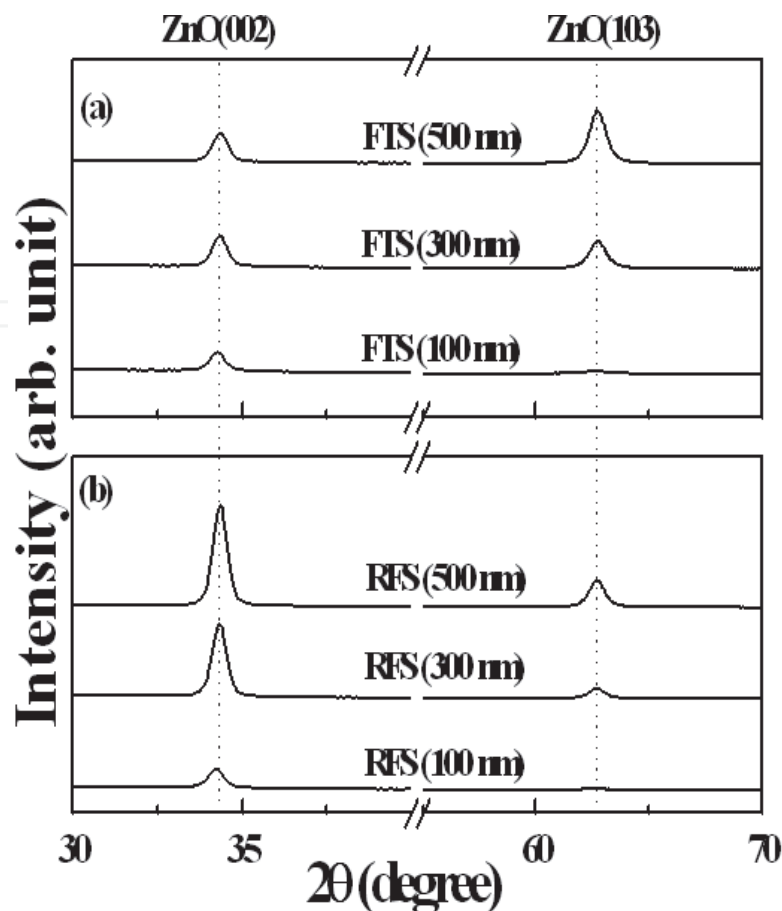


Fig. 14. X-ray diffraction patterns of the TZO thin films with thickness of 200 nm on PEN substrate under various rf-power.

like the shapes grown in vertical direction like (002) plane, as explained in Fig. 14. Generally, the thin films were condensed by vapor and atoms or molecular when the materials were deposited. At that time, some grains by the mobility decided as a function of the deposition methods and conditions were diffused, and then were moved in horizontal direction on the film surface.

However, if the applied energy for film deposition was low, the atoms with low mobility can't easily move in horizontal directions because it was frozen when the atoms were reached on the substrate. Therefore, the TZO films by FTS system shows relatively uniform surface morphology and the dense structures as shown in Fig. 16(a)-(c) while the films by the RFS system have open structures and rough surfaces contain with some pores between the grains in Fig. 16(d)-(f). The TZO film prepared by FTS system can reduce the damage on the films due to decrease the bombardment of high-energy particles such as gamma-electron. Thus, the surface roughness of the films by FTS system shows lower than that of the film by RFS system.

Among the films by FTS and RFS system, we suggest that the TZO film with 300 nm thickness prepared by FTS method can possible applied as promising substitutes for the conventional ITO film. Because the TZO film by FTS system was deposited by plasma-free sputter method with low temperature process and also has many advantages such as low resistance, high transmittance, uniform surface, cost effective production without indium component, and so on.

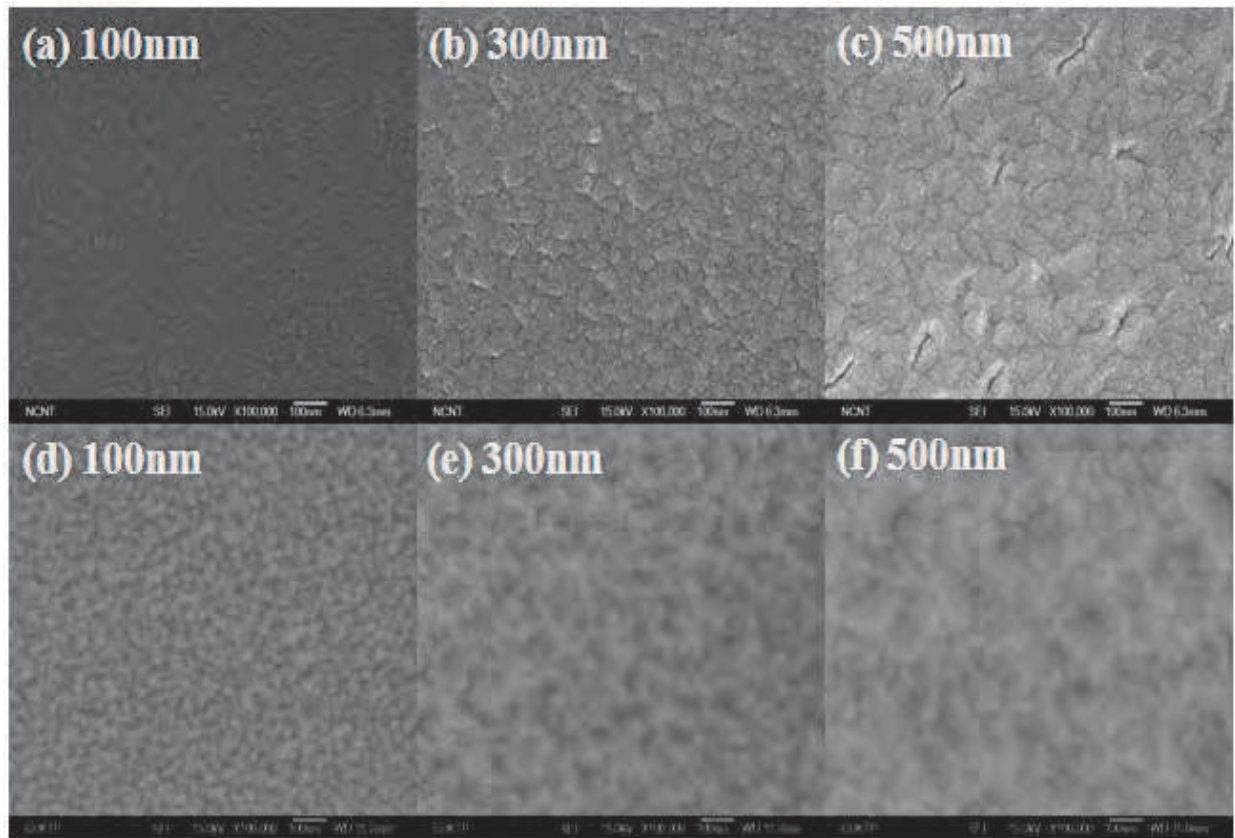


Fig. 15. SEM images of TZO films prepared by (a)-(c) FTS system and (d)-(f) RFS system with various deposition thickness.

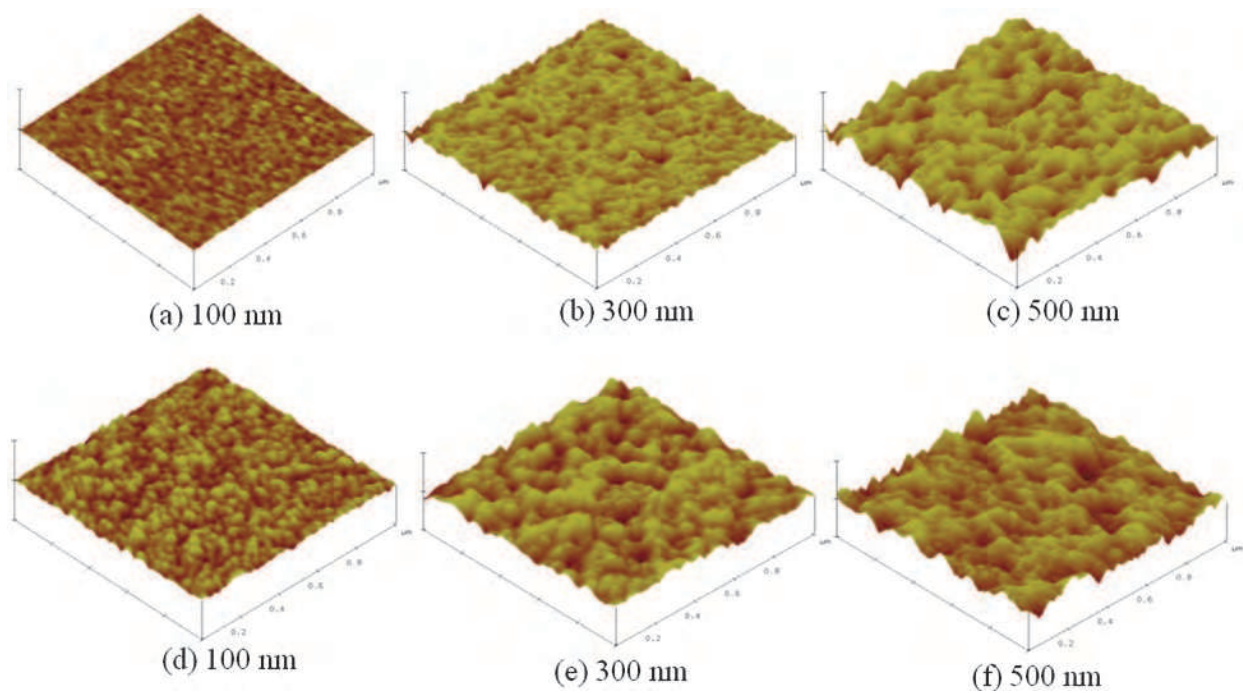


Fig. 16. AFM images of TZO films prepared by (a)-(c) FTS system and (d)-(f) RFS system with various deposition thickness.

2.5 Characterization of TCO films

2.5.1 Electrical properties

The purpose of the 4-point probe is to measure the resistivity of any semiconductor material. It can measure either bulk or thin film specimen, each of which consists of a different expression. The derivation will be shown in this tutorial. In a sheet resistance measurement, several resistances need to be considered, as shown in Fig. 17 (a). The probe has a probe resistance R_p . It can be determined by shorting two probes and measuring their resistances. At the interface between the probe tip and the semiconductor, there is a probe contact resistance, R_{cp} . When the current flows from the small tip into the semiconductor and spreads out in the semiconductor, there will be a spreading resistance, R_{sp} . Finally the semiconductor itself has a sheet resistance R_s . The equivalent circuit for the measurement of semiconductor sheet resistance by using the four-point probe is shown in Fig. 17. Two probes carry the current and the other two probes sense the voltage. Each probe has a probe resistance R_p , a probe contact resistance R_{cp} and a spreading resistance R_{sp} associated with it. However, these parasitic resistances can be neglected for the two voltage probes because the voltage is measured with a high impedance voltmeter, which draws very little current. Thus the voltage drops across these parasitic resistances are insignificantly small. The voltage reading from the voltmeter is approximately equal to the voltage drop across the semiconductor sheet resistance.

By using the four-point probe method, the semiconductor sheet resistance can be calculated:

$$R_s = F (V/I) \quad (6)$$

, where V is the voltage reading from the voltmeter, I is the current carried by the two current carrying probes, and F is a correction factor.

For collinear or in-line probes with equal probe spacing, the correction factor F can be written as a product of three separate correction factors:

$$F = F1 \cdot F2 \cdot F3 \quad (7)$$

$F1$ corrects for finite sample thickness, $F2$ corrects for finite lateral sample dimensions, and $F3$ corrects for placement of the probes with finite distances from the sample edges. For very thin samples with the probes being far from the sample edge, $F2$ and $F3$ are approximately equal to one (1.0), and the expression of the semiconductor sheet resistance becomes:

$$R_s = (\pi / \log 2)(V/I) \quad (8)$$

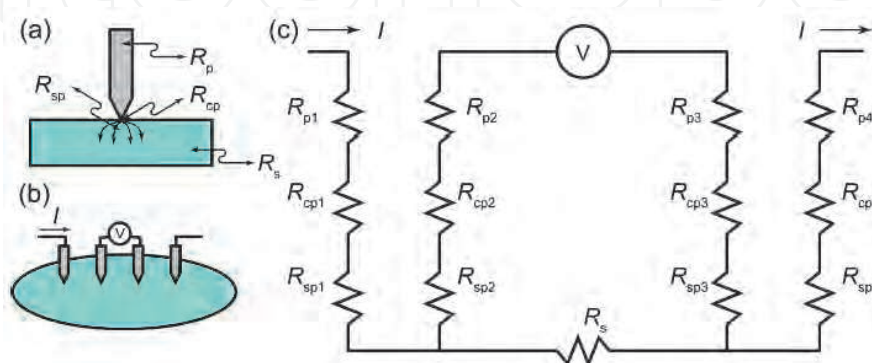


Fig. 17. 4-pin probe measurement of semiconductor sheet resistance.

The four-point probe method can eliminate the effect introduced by the probe resistance, probe contact resistance and spreading resistance. Therefore it has more accuracy than the two point probe method. For more detail the electrical property, the Hall measurement system is a complete system for measuring the resistivity, carrier concentration, and mobility of semiconductors. The system includes software with I-V curve capability for checking the ohmic integrity of the user made sample contacts. The systems can be used to characterize various materials including semiconductors and compound semiconductors (N Type & P Type) such as Si, Ge, SiGe, SiC, GaAs, InGaAs, InP, GaN, ZnO, TCOs, metals, etc., at both 300K and 77K (room temperature and liquid nitrogen temperature). An electric field from Fig. 18 and 19 is applied along the x-axis and a magnetic field is applied along the z-axis.

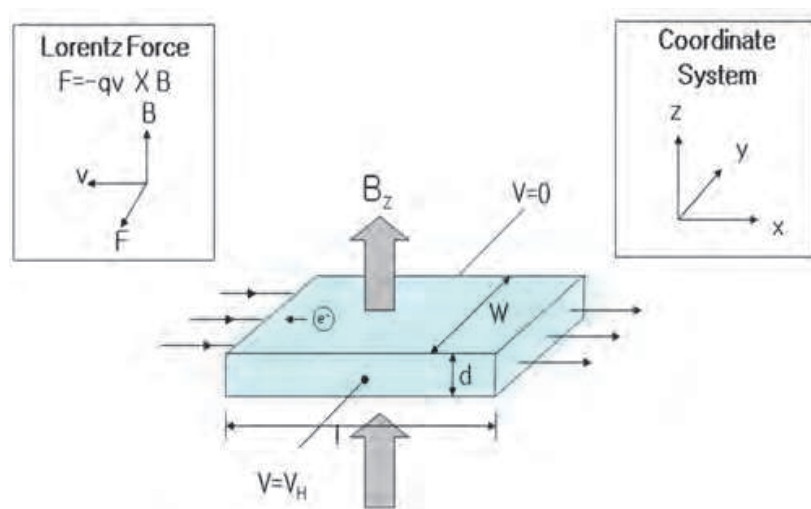


Fig. 18. Hall effects and Lorentz force.

For a p-type semiconductor sample, the Lorentz force due to the magnetic field exerts an average upward force on the holes flowing in the x-direction toward the positive y-axis which results in the accumulation of holes at the top of the sample that gives rise to a downward directed (y direction) electric field. The established electric field is called the Hall field and the voltage drop across the top and bottom of the sample is called the Hall voltage.

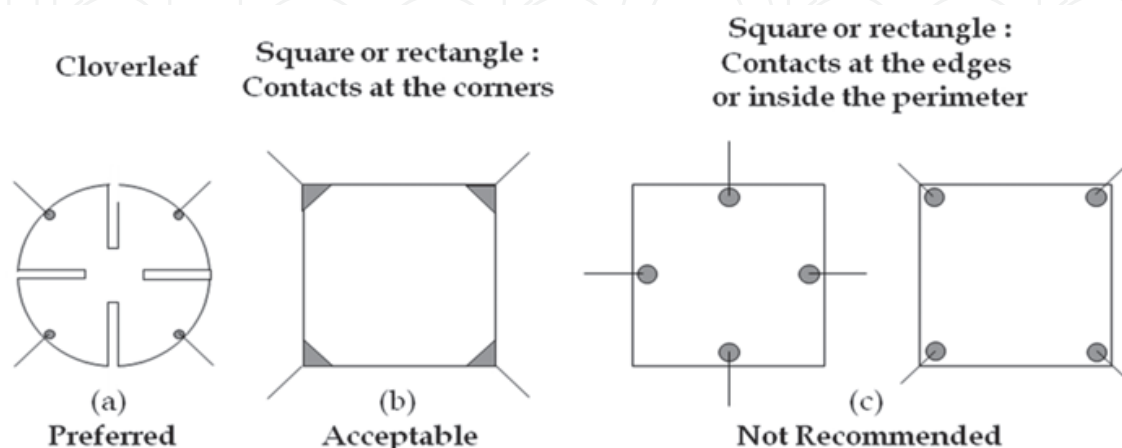


Fig. 19. Sample geometry using Van der Pauw method.

2.5.2 Optical properties

UV-VIS refers to absorption spectroscopy or reflectance spectroscopy in the ultraviolet-visible spectral region. This means it uses light in the visible and adjacent (near-UV and near-infrared (NIR)) ranges. A sample in a cuvette is exposed to light energy between 190 nm and 1000 nm. Spectrophotometry investigates the absorption of the different substances between the wavelength limits 190 nm and 780 nm (visible spectroscopy is restricted to the wavelength range of electromagnetic radiation detectable by the human eye, that is above ~360 nm; ultraviolet spectroscopy is used for shorter wavelengths). In this wavelength range the absorption of the electromagnetic radiation is caused by the excitation (i.e. transition to a higher energy level) of the bonding and non-bonding electrons of the ions or molecules. A graph of absorbance against wavelength gives the sample's absorption spectrum. Modern spectrophotometers draw this automatically. The measured spectrum is continuous, due to the fact that the different vibration and rotation states of the molecules make the absorption band wider. Certain parts of an organic molecule will absorbance some of this energy to create peaks on a spectrum for quantitative (primarily) and qualitative Analysis. The original UV-Vis specs were made as *DOUBLE-BEAM* units to correct for noise, drift and other Instabilities. Over 20 years ago, the well-known leaders in the analytical instrument markets; Beckman & Perkin-Elmer; began to focus on a line of "Stable-Beam" *SINGLE-BEAM* Instruments. Spectrophotometry is used for both qualitative and quantitative investigations of samples. The wavelength at the maximum of the absorption band will give information about the structure of the molecule or ion and the extent of the absorption is proportional with the amount of the species absorbing the light. Quantitative measurements are based on Beer's Law (also known as "Lambert-Beer Law" or even "Bouguer-Lambert-Beer Law") which is described as follows:

$$A = ec l \quad (9)$$

, where A = absorbance [no units, because it is calculated as $A = \log_{10}(I_0/I)$, where I_0 is the incident light's intensity and I is the light intensity after it passes through the sample];

e = molar absorbance or absorption coefficient [in $\text{dm}^3 \text{mol}^{-1} \text{cm}^{-1}$ units];

c = concentration (molarity) of the compound in the solution [in mol dm^{-3} units];

l = path length of light in the sample [in cm units].

2.5.3 Structural properties

Atomic force microscope (AFM) provides a 3D profile of the surface on a nanoscale, by measuring forces between a sharp probe (<10 nm) and surface at very short distance (0.2-10 nm probe-sample separation). The probe is supported on a flexible cantilever. The AFM tip "gently" touches the surface and records the small force between the probe and the surface. The probe is placed on the end of a cantilever (which one can think of as a spring). The amount of force between the probe and sample is dependent on the spring constant (stiffness) of the cantilever and the distance between the probe and the sample surface. This force can be described using Hooke's Law:

$$F = -k x \quad (10)$$

, where F is force, k is spring constant, and x is cantilever deflection.

If the spring constant of cantilever (typically ~0.1-1 N/m) is less than surface, the cantilever bents and the deflection is monitored. This typically results in forces ranging from nN(10^{-9}) to μN (10^{-6}) in the air. If the tip was scanned at a constant height, a risk

would exist that the tip collides with the surface, causing damage. Hence, in most cases a feedback mechanism is employed to adjust the tip-to-sample distance to maintain a constant force between the tip and the sample. Traditionally, the sample is mounted on a piezoelectric tube that can move the sample in the z direction for maintaining a constant force, and the x and y directions for scanning the sample. Alternatively a 'tripod' configuration of three piezo crystals may be employed, with each responsible for scanning in the x, y and z directions. This eliminates some of the distortion effects seen with a tube scanner. In newer designs, the tip is mounted on a vertical piezo scanner while the sample is being scanned in X and Y using another piezo block. The resulting map of the area $z = f(x,y)$ represents the topography of the sample.

The AFM can be operated in a number of modes, depending on the application. In general, possible imaging modes are divided into static (also called contact) modes and a variety of dynamic (or non-contact) modes where the cantilever is vibrated.

Contact Mode AFM: (repulsive VdW) When the spring constant of cantilever is less than surface, the cantilever bends. The force on the tip is repulsive. By maintaining a constant cantilever deflection (using the feedback loops) the force between the probe and the sample remains constant and an image of the surface is obtained from Fig. 20.

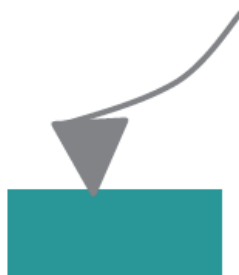


Fig. 20. Schematic of contact mode AFM.

Intermittent Mode (Tapping): The imaging is similar to contact. However, in this mode the cantilever is oscillated at its resonant frequency. The probe lightly "taps" on the sample surface during scanning, contacting the surface at the bottom of its swing. By maintaining constant oscillation amplitude a constant tip-sample interaction is maintained and an image of the surface is obtained from Fig. 21.

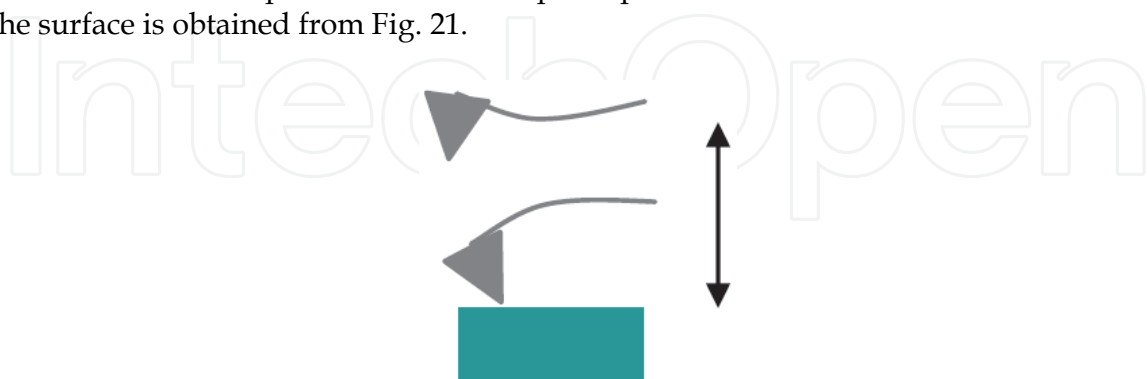


Fig. 21. Schematic of tapping mode AFM with oscillation amplitude of 20-100 nm.

Non-contact Mode: (attractive VdW) The probe does not contact the sample surface, but oscillates above the adsorbed fluid layer on the surface during scanning. (Note: all samples unless in a controlled UHV or environmental chamber have some liquid adsorbed on the

surface). Using a feedback loop to monitor changes in the amplitude due to attractive VdW forces the surface topography can be measured from Fig. 22.

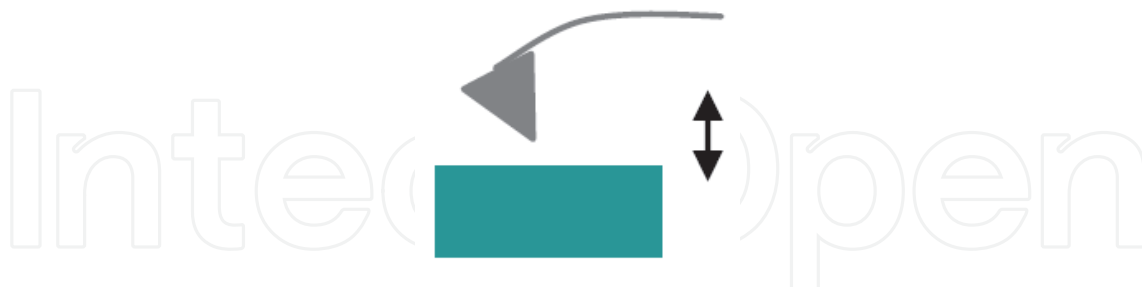


Fig. 22. Schematic of non-contact mode AFM.

The SEM has many applications across a multitude of industry sectors. It can produce extremely high magnification images (up to 200000 times) at high resolution up to 2 nm combined with the ability to generate localised chemical information (EDX). This means the SEM/EDX instrument is a powerful and flexible tool for solving a wide range of product and processing problems for a diverse range of metals and materials. A finely focused electron beam scanned across the surface of the sample generates secondary electrons, backscattered electrons, and characteristic X-rays. These signals are collected by detectors to form images of the sample displayed on a cathode ray tube screen. Features seen in the SEM image may then be immediately analyzed for elemental composition using EDS or WDS. Secondary electron imaging shows the topography of surface features a few nm across. Films and stains as thin as 20 nm produce adequate-contrast images. Materials are viewed at useful magnifications up to 100,000 times without the need for extensive sample preparation and without damaging the sample. Even higher magnifications and resolution are routinely obtained by our Field Emission SEM. Backscattered electron imaging shows the spatial distribution of elements or compounds within the top micron of the sample. Features as small as 10 nm are resolved and composition variations of as little as 0.2% determined. Data output is generated in real time on the CRT monitor. Images and spectra can be printed here, recorded on CD-ROM and/or emailed for insertion into your own reports.

Diffraction effects are observed when electromagnetic radiation impinges on periodic structures with geometrical variations on the length scale of the wavelength of the radiation. The inter-atomic distances in crystals and molecules amount to 0.15–0.4 nm which correspond in the electromagnetic spectrum with the wavelength of x-rays having photon energies between 3 and 8 keV. Accordingly, phenomena like constructive and destructive interference should become observable when crystalline and molecular structures are exposed to x-rays. Firstly, the geometrical constraints that have to be obeyed for x-ray interference to be observed are introduced. Secondly, the results are exemplified by introducing the $\theta/2\theta$ scan, which is a major x-ray scattering technique in thin-film analysis. Thirdly, the $\theta/2\theta$ diffraction pattern is used to outline the factors that determine the intensity of x-ray reflections. We will thereby rely on numerous analogies to classical optics and frequently use will be made of the fact that the scattering of radiation has to proceed coherently, i.e. the phase information has to be sustained for an interference to be observed. The selective perception of certain subsets of crystallites in a $\theta/2\theta$ scan is visualized in Fig. 23.

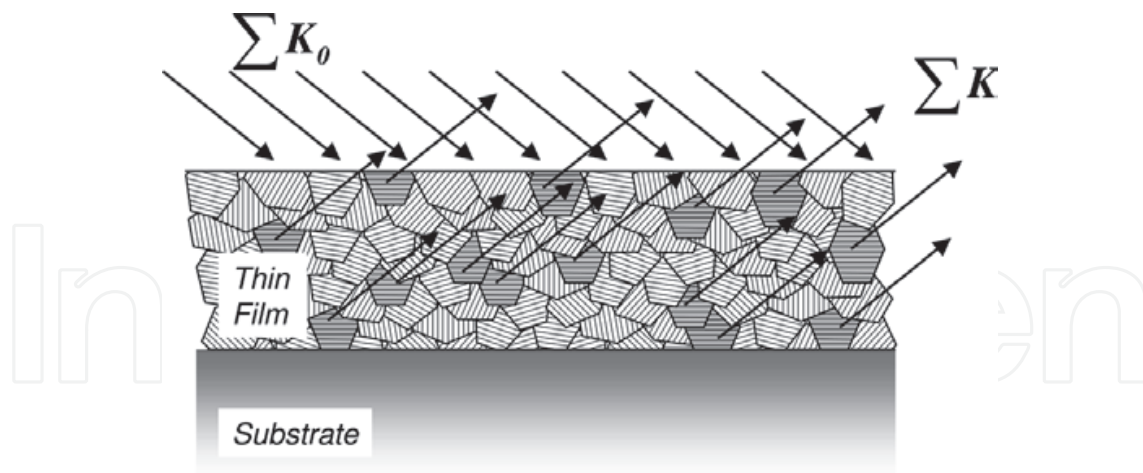


Fig. 23. Selection principle for exclusive measurement of surface-parallel lattice planes in a $\theta/2\theta$ scan.

2.6 Novel materials

2.6.1 Organic conductors

The most commonly used polymeric hole conductor is PEDOT:PSS, sold by H.C. Starch as Baytron®P. And it acts as the anode and normally deposited from an aqueous dispersion. This polymer is water soluble, and hence can be used as a transparent anode. PEDOT:PSS belongs to the class of semiconducting polythiophenes. High conductivity PEDOT:PSS is considered as the most relevant polymer to replace TCOs and has been successfully introduced in organic solar cells and/or OLEDs as transparent bottom electrode, located directly on the substrate, or as transparent top electrode. In an experiment to prove the principle, Arias et al. have shown that a poly(p-phenylene vinylene) (PPV) layer sandwiched between PEDOT:PSS and Al forms a photovoltaic device independent of whether a polymer or a metal is deposited as the final layer. To overcome resistive losses across the anode, the conducting polymer has been deposited by spin-coating or screen printing on an underlying metal grid with gold or silver.

The development of water-soluble transparent conducting-doped polyaniline(PANI), enabled the first fabrication of an “all plastic” polymer light emissive devices(PLEDs). The metallic emeraldine salt form of PANI was prepared by protonation with camphor-sulfonic acid(CSA), yielding a conducting PANI complex soluble in common organic solvents. The optical transmission(200–2000 nm), sheet resistance and work functions of ITO(100 Ω/\square), ITO(12 Ω/\square), ZnO, AZO and polyaniline(PANI) films were measured as shown in Table 1.(Guan et al., 2009)

And also, the effect that the dopant, solvent, and type of conducting polymer have on the device performance and lifetime with and without ITO in the device structure were determined. The device performance is improved more markedly with polymer-based dopants independent of conductivity, solvent, or type of conducting polymer. Moreover, the device lifetime is substantially improved when ITO is eliminated from the device structure. In Table 2, we list the conducting polymer anodes, dopant type, solvent, conductivity, and external quantum efficiency (QE) at 7 V, radiance at 7 V before aging, and radiance at 7 V after 200 h of aging.

Film	Thickness/ nm	Sheet resis- tance/ $(\Omega \cdot \square^{-1})$	Work func- tion/eV	Transmittance(%) (at 1.54 μm)
ITO(12 Ω/\square)	~180	~12	4.5 \pm 0.1	35
ITO(100 Ω/\square)	~35	~100	4.4 \pm 0.1	85
ZnO	~400	~10000	—	88
AZO	~130	~400	5.1 \pm 0.1	30
PANI	~110	~800	4.8 \pm 0.1	39

Table 1. Relevant properties of transparent conducting films on glass substrates.

Dopant-polymer/ solvent ^b	$\sigma(\Omega \text{cm})^{-1}$	%QE at 7 V	L (cd/m ²) at 7 V fresh	L (cd/m ²) 200 h at 7 V
PSS-PAni/H ₂ O	0.1	1.4	4000	30 w/ITO ^c
PSS-PAni/NMP	0.1	1.0	1500	
PAPS-PAni/H ₂ O	discontinuous	1.1	1200	
APS-PAni/FA	100	0.4	3000	
CSA-PAni/FA	200	0.3	1000 w/Au	50 w/Au
PSS-PEDT/H ₂ O	2	1.3	1800	
			4000 w/ITO	30 w/ITO
			300 w/Au	35 w/Au
			180 none	60 none

Table 2. Performance of PLEDs with various polymer anodes ~100 nm MEH-PPV.

The two types of conducting polymers studied were PANi and polyethylenedioxythiophene (PEDT). The PANi materials were doped with two different polymer dopants, polystyrenesulfonic acid and polyacrylamidopropanesulfonic acid, and two monomer dopants, amidopropanesulfonic acid and camphor sulfonic acid, for comparison. Average lifetime behaviors on samples with and without ITO are shown in Fig. 24. (Carter et al., 1997) In general, the brightest diodes with the higher current densities decayed the most rapidly; however, the diodes with the ITO in the device structure continued to decay more rapidly even when the current densities were below that of the devices without ITO in the structure. In the next 200 h, the light output in non-ITO devices decayed less than 20% while the ITO-based diodes lost nearly another order of magnitude. This effect is also observed if the diodes are aged at a much lower dc voltage ~4 V and current density. These results indicate that the long-term device failure is accelerated by the presence of ITO, caused by photo-oxidation of the light-emitting polymer via oxygen evolved from the ITO. The mechanism for the short-term aging is currently under further investigation.

2.6.2 Nanometals

Since Pt has a very high work function of about 5.6 eV, it could strongly enhance hole injection. However, in order to use for TCO films, Pt must be very thin to be transparent, and it would be deposited on, e.g., the conventional ITO. Malliaras et al. have shown that a

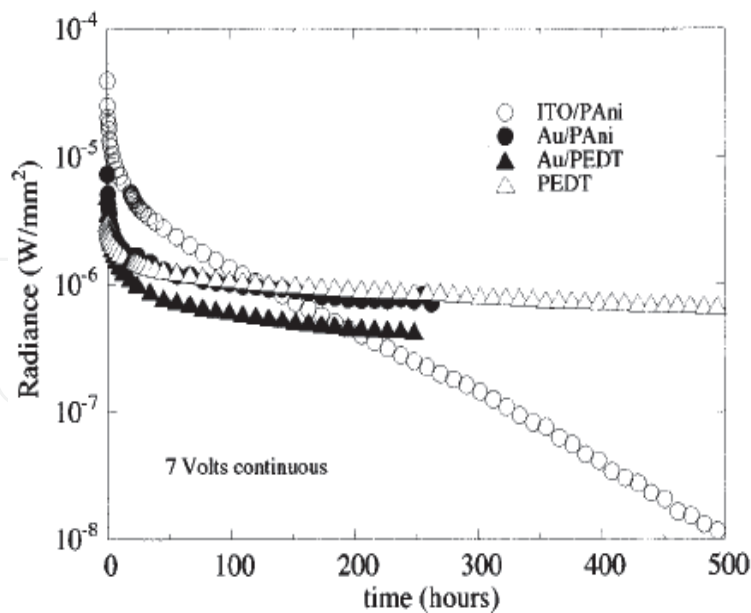


Fig. 24. Radiance lifetime studies for different PLED device structures. Devices without ITO in the device structure have improved long lifetime behavior. $1 \text{ W/mm}^2 = 7.3 \times 10^7 \text{ cd/m}^2$.

thin layer ($\leq 10 \text{ \AA}$) of Pt on ITO enhances hole injection by up to a factor of 100 relative to the uncoated ITO. In order to investigate the properties of the multilayer TCO, a sandwich structure of ITO(50 nm)/Au(5 nm)/ITO(45 nm) (IAI) multilayer films compared with conventional ITO film were analyzed on glass substrates without intentional substrate heating for application such as OLEDs, STN-LCDs, gas sensor, solar cells, and so on. The electrical properties of the IAI and ITO films evaluated with Hall Effect measurements were measured. Although ITO/Au/ITO films have a lower mobility than ITO single-layer films, they have a lower resistivity as shown in Table 3. (Kim et al., 2007) The decrease in the resistivity of the IAI films may be caused by the increase in the carrier density of the IAI films, which results from the presence of the Au interlayer. However, the ITO/Au/ITO films have a lower mobility than the ITO single-layer films, which suggesting that the two interfaces between the ITO and Au film may act as a barrier to carrier movement.

	ITO	ITO/Au/ITO
Carrier density	1.8	220
Mobility	140.8	47.4
resistivity	40.2	0.5

Table 3. The comparison of the carrier density ($\times 10^{19}/\text{cm}^3$), mobility (cm^2/Vs) and resistivity ($\times 10^{-4} \Omega \cdot \text{cm}$) of the ITO and ITO/Au/ITO films.

Transmittance and sheet resistance values at ITO/Ag/ITO structure are found mainly dependent on the Ag film thickness; whereas the wavelength range at which the maximum transmittance is controlled by the ITO film thickness. (Guillen et al., 2009) Lowest sheet resistance at ITO/Ag/ITO structure have been obtained below 6 ohm/sq at Ag film thickness above 10 nm and ITO layers thickness in the 30-50 nm range. Choi *et. al* investigated the effects of the post-annealing temperature on the TCO film properties with ITO/Ag/ITO structure. (Choi et al., 1999) The properties of multilayer films, especially the

optical and electrical properties, depended dominantly on the characteristics of Ag film. The morphology and structure of very thin Ag film were sensitive to the deposition temperature. The Fig. 25 shows the optical transmission spectra of Ag films deposited for 70 s at 25, 100 and 200°C, which shows various transmittances from 20% to 80% in visible light range. The spectrum of 200°C shows the lowest transmittance. The color of the film was dark violet, but the others were blue. Light scattering by the rough surface reduced the transmittance. Substrate heating during Ag film deposition led to the same effect on the multilayer film. When Ag film deposition temperature was 200°C in the preparing process of multilayer, both visible transmittance and conductivity decreased.

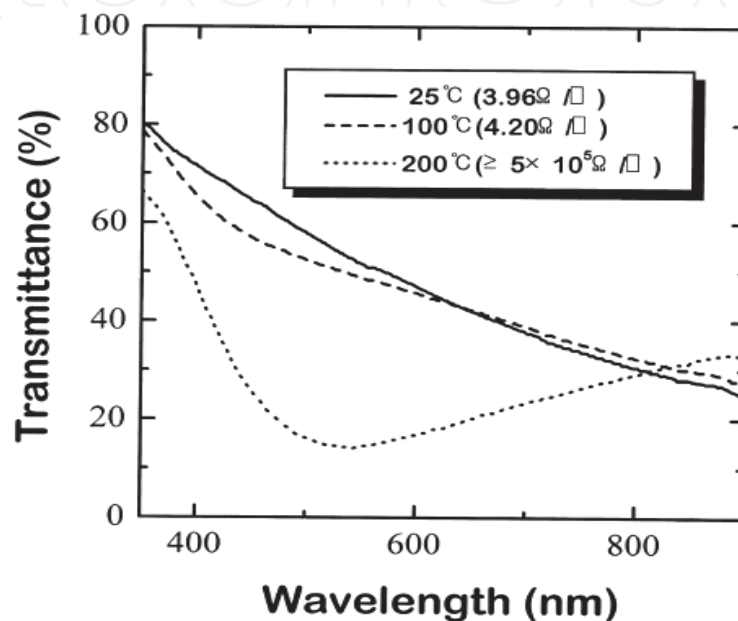


Fig. 25. Optical transmission spectra and sheet resistance of Ag thin films deposited on glass at 25, 100, and 200°C. Deposition time was 70 s.

Their micrographs of these films are shown in Fig. 26. Because substrate heating causes low nucleation density, we obtained island structure films at 200 °C, where a continuous film had not formed yet.

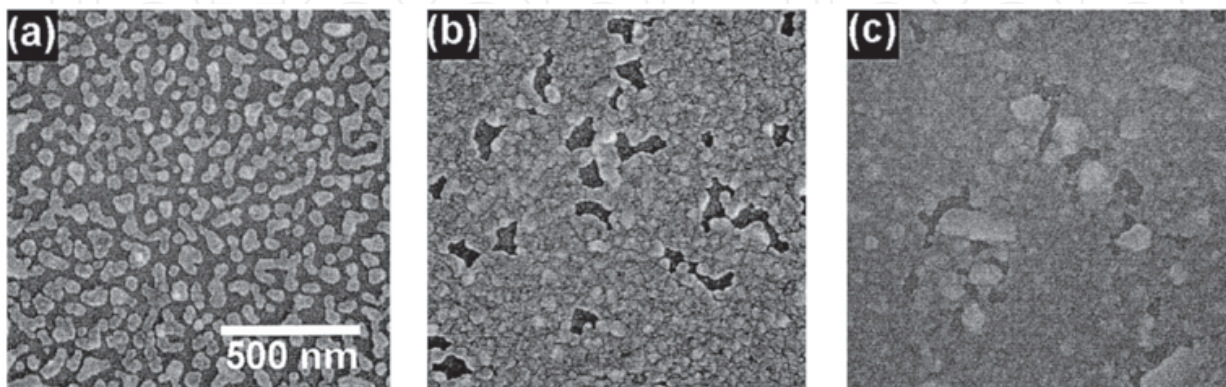


Fig. 26. SEM micrographs of Ag thin films deposited on glass at (a) 25, (b) 100, and (c) 200°C. Deposition time was 70 s.

2.6.3 Carbon nanotubes and graphene

Electrode materials for the most important properties are very high conductivity. Use materials with high conductivity and relatively small amount when using the material to lower the price, and the concentration of material to help penetration of the transparent electrode is connected directly. The following requirements are important to low processing temperatures, low manufacturing cost and a uniform printing properties, adhesion with the substrate, such as external friction by abrasion, weathering and chemical resistance of various organic solvents, etc. are needed. The conductive ink materials which is currently used or has been studied, give a similar examples, such as; conductive polymer solution, liquid dispersed in metal nano-particles, carbon nanotubes(CNT) composite materials, as shown in Fig. 27.

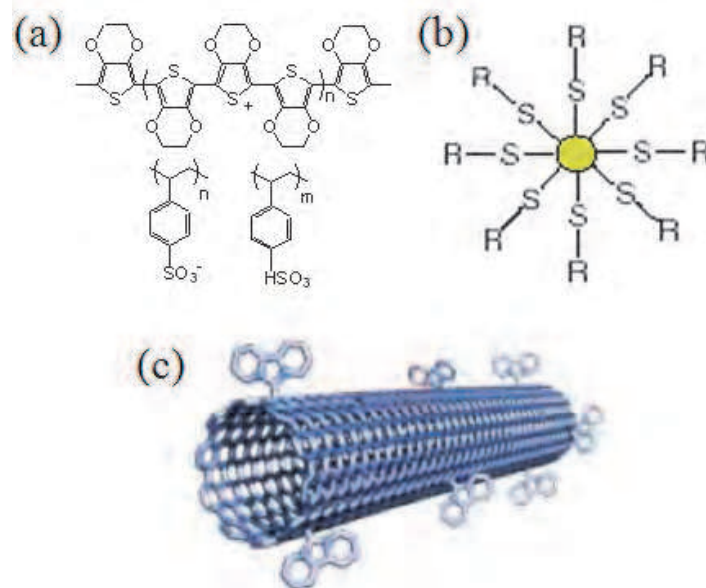


Fig. 27. Conductive ink materials. (a) PEDOT:PSS, (b) metal nano particle, and (c) surface modified carbon nanotube.

Metal nano-particles have enough stocks as high conductivity. But, to remove the dispersion agent that the wrists are used to distribute these materials, relatively high firing temperatures (>150 °C) and the expensive production costs are required. Therefore, there can be a little more low-cost manufacturing process for the development of distributed and can lower the sintering temperature is necessary to develop the dispersion agent. Conductive polymer dispersion in high and low process temperature, the easy one because the fairness, conductivity is very low (1~10 S/cm) compared to the metal nano-particles. Therefore, the research on polymer material with high conductivity is needed. Because the CNT dispersion solutions are difficult to disperse in common solvents, Modified CNT surface and dispersed in a solvent such as water and ink are used. CNT is lower than the relatively high conductivity of metal nanoparticles (100~1000 S/cm) and low processing temperature (100 °C), but because of being researched in recent long-term stable dispersion of CNT getting more difficult, and studies are needed.

Dai Nippon Printing (DNP) Co., Ltd. and Fujifilm Co. have developed a new method, which can directly coating the metal grid using fine pattern printing method by Ag nano-ink. Fig. 28(a) shows the TCO electrode of a nano-mesh type developed in DNP Co., Ltd. and

Fujifilm Co. Because the films of DNP Co., Ltd. can form the uniform pattern at only necessary parts, it can be reduced the unnecessary deposition and etching process during ITO fabrication. And also, Fujifilm Co. of Fig. 28(c) has developed a new type of electrode, which can control the resistivity from $0.2 \Omega/\text{cm}^2$ to thousands Ω/cm^2 using Ag pattern of mesh type on PET substrate and organic/inorganic conductive materials. U.S. venture cambrios Co. released the transparent conductive ink as a wet coating, which contains soluble metal nano-wire, as shown in Fig. 28(b). The image shows the dispersed shape on a substrate at Ag nanowires fabricated in Cambrios Co. uniformly distributed wire of the nano-scale film can form the film as a type of mesh, has excellent permeability and high resistivity. And also, it has advantage which can be directly coated at room temperature. And also, Toray and Cimma Co. in Fig. 28(d) developed the transparent electrode with transmittance over 80% using self-aligning mechanism of silver nano-particles.

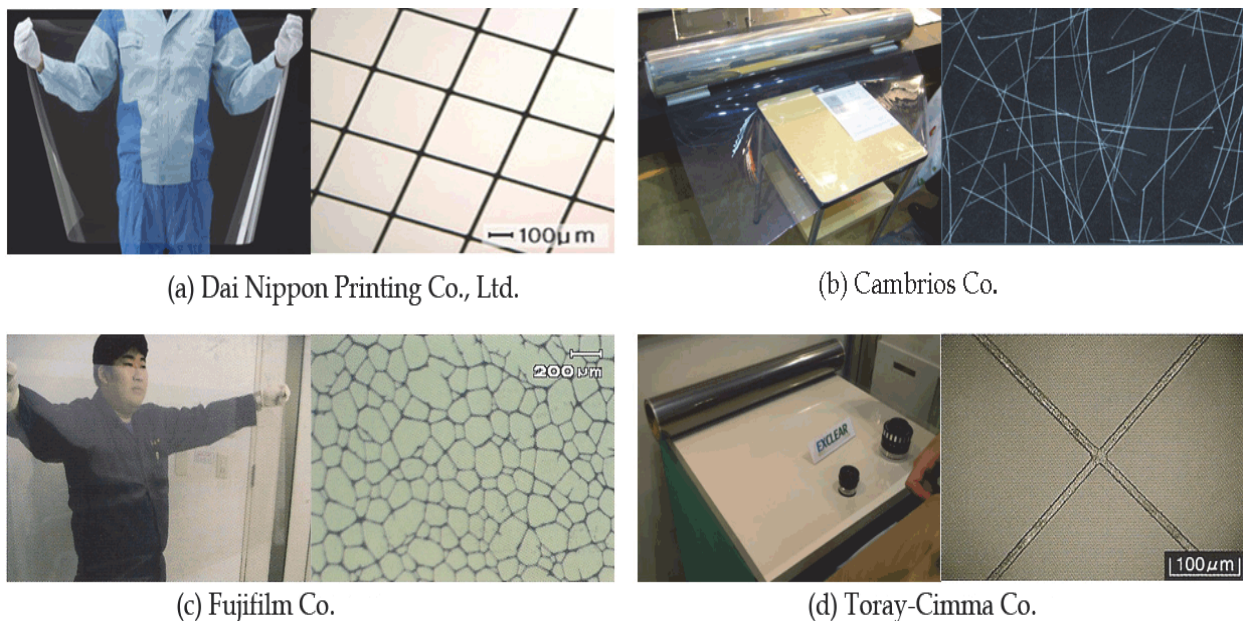


Fig. 28. Transparent electrodes of nano-mesh type.

2.7 TCOs for flexible OLEDs

In most case, OLEDs have been traditionally fabricated on glass substrate, however, there OLEDs have several disadvantage for certain applications such as portable communication display, because the glass substrate is very fragile, heavy and non-flexible. Flexible OLEDs (FOLEDs) using the plastic substrate are growing attention, because a plastic substrate can be overcome disadvantages of a glass substrate. These devices provide the ability to conform, bend or roll-up display into any shape. (Gu et al., 1997) This means that FOLEDs may be laminated onto an automotive windshield, or an aircraft cockpit et al. However, the low thermal stability of a plastic substrate ($T_g=80 \text{ }^\circ\text{C}$) is difficult the process for making transparent conducting electrode, indium tin oxide (ITO), and TFT. These materials are necessary for the high temperature $\geq 200 \text{ }^\circ\text{C}$. Conventional FOLEDs are fabricated the polymer materials. (Gustaffson et al., 1993; He & Kanicki, 2000) Y. Zhang and S. R. Forrest were suggested that thermal deposited organic thin films have the general flexibility property by the van der waals force between aromatic atoms-to-atoms. (Zhang

& Forrest, 1993) Since these results were reported, G. Gu shows that a conventional small molecule organic materials can be successfully fabricated FOLEDs.(Gu et al., 1997) As FOLEDs attempted cyclic bending test, the electrode layer consist of an inorganic materials, such as ITO and metal cathode, had cracked surface because an inorganic layers are brittle materials. Under mechanical stresses, micro crack and propagation of existing pinholes will be significantly reductive such as the contact properties between an organic and electrode layer. In this work, we report that FOLEDs in the sequence of ITO, organic materials, and aluminum(Al) deposited on the PET substrate by using low temperature process. The current density and brightness property of FOLEDs were investigated as a function of the radius of variation bending test. To investigate change of the surface in an inorganic electrode after the mechanical flexibility test, scanning electron microscope (SEM) was used.

For fabricating the FOLEDs, an ITO, N,N'-diphenyl-N,N'-bis(3-methylphenyl)-1,1'-diphenyl-4,4'-diamin (TPD), tris-(8-hydroxyquinoline) aluminum (Alq₃), and Al were used as an anode, HTL, emitting material layer(EML), and cathode, respectively. The ITO electrode was deposited on top of the PET substrate by RF-magnetron sputtering at room temperature. The ITO target is an alloy of In₂O₃ (90 %) and SnO₂ (10 %) by weight, with 99.99 % purity. The base pressure of the sputtering chamber was 5×10⁻⁶ torr, and the sputter deposition pressure of the ITO film was 6×10⁻³ torr with Ar and O₂ flows regulated by mass flow controller at 25 sccm and 1 sccm, respectively. The r. f. sputtering power was 50 W, resulting in a deposition rate of 2.8 nm/s. The sheet resistance of 150 nm thick-deposited the ITO film is 50 Ω/sq, and its transmission was 90 % at the wavelength of 513 nm. To optimized properties of the sputter deposited electrode, ITO surface was treated by O₂ plasma at 2×10⁻¹ torr for 60 sec.(Ishii et al., 2000) The organic materials TPD and Alq₃ were deposited as thickness of 60 nm and 40 nm, respectively, at the deposition rates of 1.0-1.5 Å/s on the PET/ITO substrate. After the deposition of organic layer, the Al cathode layer was deposited as the thickness of 100 nm at the deposition rates 10 Å/s by thermal evaporation. The performance of FOLEDs was measured after repeated bending each 100 times per samples at radius as a function of various bending test range. To analyze electrical property and brightness intensity of FOLEDs, we measured by Keithly 2400 electrometer, Si photodiode and Keithly 485 picoammeter. The sheet resistance of ITO after the bending test were measured by four-point probe, and surface morphology of ITO, organic films, and Al layer after bending test were observed by SEM(FEI company, XL30 ESEM-FEG).

Fig. 29(a) and 29(b) shows the change of current density-voltage (J-V) and brightness-voltage (B-V) characteristics for radius of curvature. The bent FOLEDs at radius of 19 mm, 16 mm, 13 mm, 10 mm, and non bending were referred to as FOLED(19), FOLED(16), FOLED(13), FOLED(10), and FOLED(0), respectively. In Fig. 29(a), the turn-on voltage of FOLED(0), FOLED(19), FOLED(16), FOLED(13), and FOLED(10) were observed at 9 V, 10 V, 10 V, 15 V, and 17 V, respectively. As the given voltage, the current density and the brightness of bent FOLEDs were substantially lower than those of the control device. The J-V and B-V properties of FOLED(19) were analogous with FOLED(0). FOLED(16) showed similar current density to FOLED(19), however, this device inferior maximum bright intensity (1440 cd/m²) than FOLED(0) (1900 cd/m²). Further decrease of the radius to 13 mm and 10 mm resulted in reduce J-V and B-V characteristics of FOLEDs.

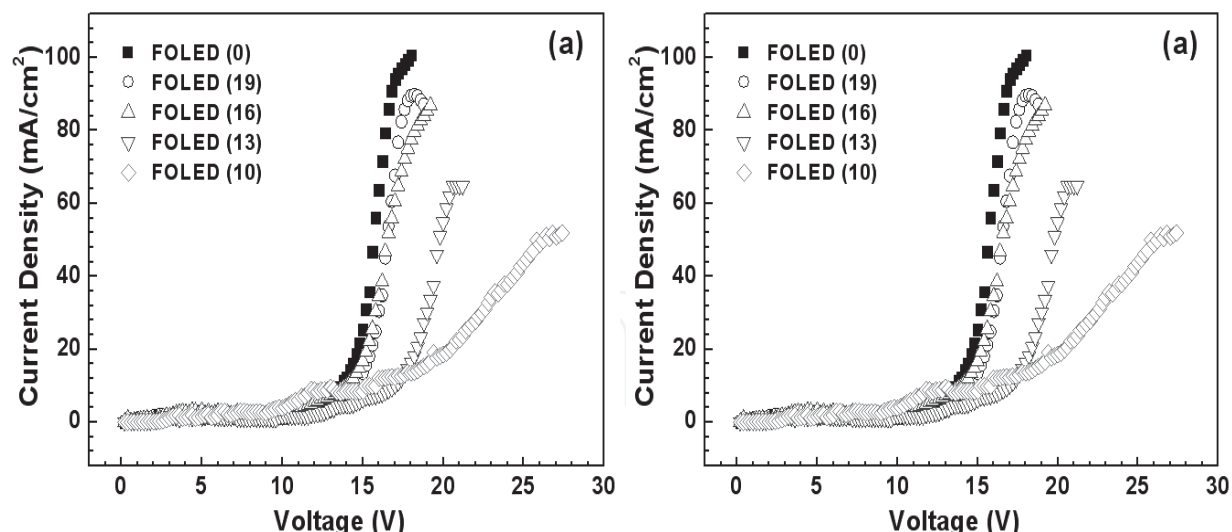


Fig. 29. (a) Current density versus voltage (J-V) and (b) brightness ver. voltage (B-V) curves of the bent FOLEDs at radius of 19 mm, 16 mm, 13 mm, 10 mm, and non bending.

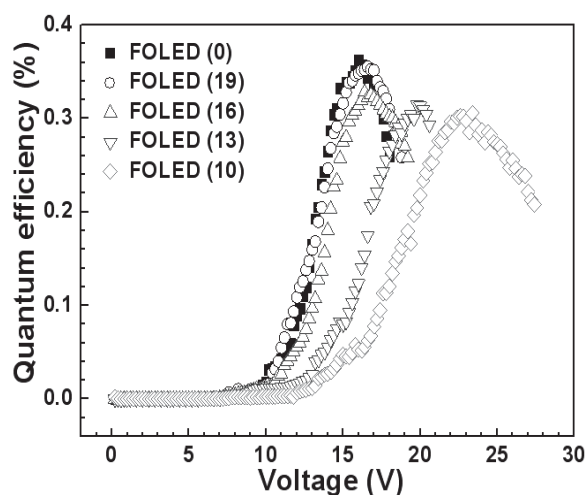


Fig. 30. Quantum efficiency ver. voltage (I-V) curves of the bent FOLEDs at radius of 19 mm, 16 mm, 13 mm, 10 mm, and non bending.

Fig. 30 shows external quantum efficiency of bent FOLEDs. FOLED(0), FOLED(19), and FOLED(16) showed maximum quantum efficiency of $\sim 0.35\%$ at 16 V. FOLED(13) and FOLED(10) have lowered quantum efficiency of 0.31% and 0.30% at 20 V and 23 V, respectively, than the other FOLEDs. As the radius of bending test decreased, the reduction of device properties, such as current density, brightness, and quantum efficiency is thought that the contact property between the layers was decreased because of mechanical stress by the bending test of FOLEDs. To measure changes of the sheet resistance after the bending test of ITO films, four point probe was observed (Fig. 31). The ITO films were deposited on the PET substrate and then ITO coated substrates were operated bending test (100 times) with various range of 19 mm, 16 mm, 13 mm, and 10 mm. The bent ITO with 19 mm showed analogous sheet resistance ($62 \Omega/\square$), with the control ITO ($50 \Omega/\square$). However, the sheet resistance of bent ITO increased as the radius of bending test decreased when the radius of bending test ≤ 16 mm. Since increased the sheet resistance of bent ITO, FOLED(13) and

FOLED(10) were thought to have a lower electric and brightness properties than FOLED(0). Although, the sheet resistance of 16 mm bent ITO is $230 \Omega/\square$, this value is sufficiently small for using electrode in OLEDs. (Gu et al., 1996)

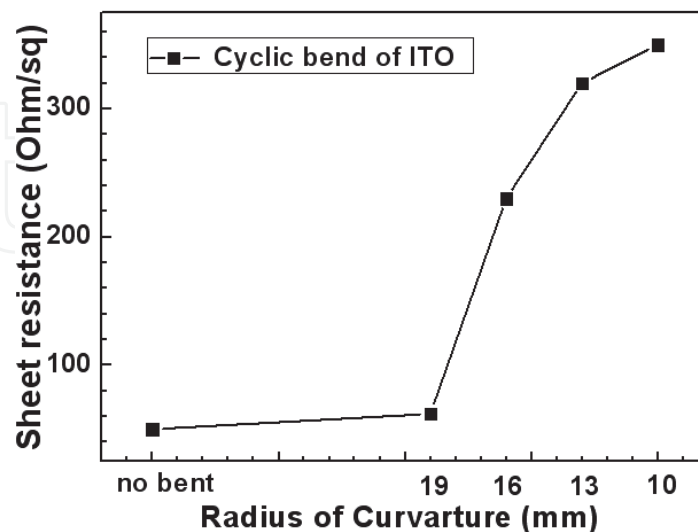


Fig. 31. Changes of the sheet resistance after the bending test of ITO films.

Fig. 32 showed the SEM images of the ITO surface as a function of the variation radius of curvature. The crack phenomenon of bent ITO was appeared from the lowered radius of bending test ≤ 16 mm. The ITO for the bending test at 13 mm and 10 mm radius showed the rough surface and a large amount of crack from the whole area. In our case, the bent ITO at 16 mm, 13 mm, and 10 mm have the hasty reductive properties, such as sheet resistance and surface morphology.

In this result, the reasons for reduced properties of bent FOLEDs are follows. Firstly, the bent FOLEDs have lowered device characteristics, such as increased driving voltage and decreased luminance property, because of the increase resistance of bent ITO by a bending test in radius of below 16 mm. (Chen et al., 2002) Secondly, many attempts have been focused on interface property between an organic and electrode layer. The OLEDs using the ITO anode with smooth surface have shown superior device properties, as lower turn-on voltage and higher luminescent efficiency, because these devices are improved contact property. In this study, the bent FOLEDs have shown inferior device performance because rough surface of the bent ITO was decreased contact property in the interface between the TPD organic layer and ITO electrode. (Kwon et al., 2002) In conclusions, we fabricated FOLEDs with an ITO anode, a TPD hole transport layer, an Alq_3 emitting layer, and an Al cathode deposited on the PET substrate and studied FOLEDs characteristics after bending test at various radiuses of 10 mm, 13 mm, 16 mm, and 19 mm. The performance of FOLEDs with lowered radius (≤ 16 mm) was decreased the device properties, and increased the sheet resistance of bent ITO. These devices showed the crack phenomena and rough surface in the ITO and Al inorganic layers. In our experiment, the optimum radius of bending test was 19 mm. When FOLEDs was bent at 19 mm radius, inorganic layer, ITO and Al, cannot show the crack phenomena. The electrical property and brightness efficiency of FOLED(19) were similar with the control device. In this result was suggested that the performance of the bent FOLEDs was affected significantly by the crack phenomenon of an inorganic layer and increased sheet resistance of bent ITO.

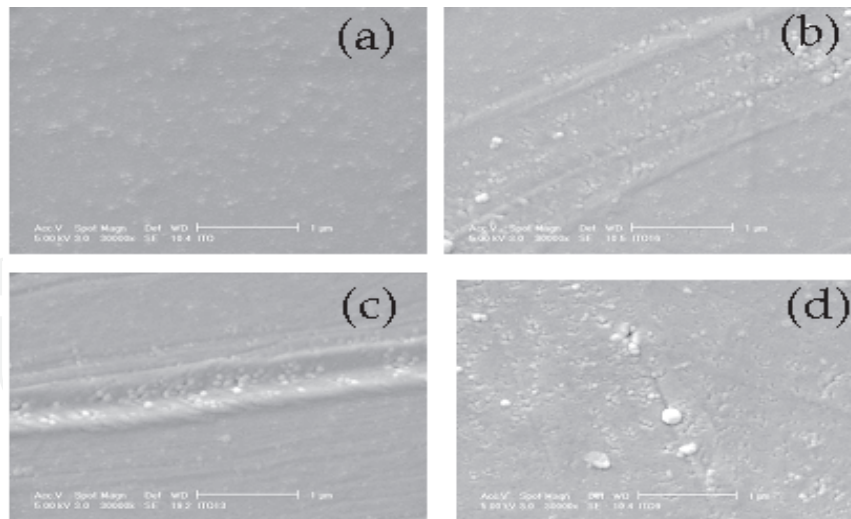


Fig. 32. SEM images of the ITO surfaces (a) without bending and with bending as a function of the variation radius of curvatures in (b) 16 mm, (c) 13 mm, and (d) 10 mm.

3. Conclusion

In fabricating OLED devices, ITO film among the TCO films is widely used as an anode layer, because of its high transparency in the visible light range, low conductivity, and high work function, etc. However, indium in ITO has a tendency to diffuse into the emissive polymer layer under device operation, which may in turn influence the quantum efficiency and lifetimes of OLEDs. In addition, it is known that the performance of ITO-based polymer LEDs is highly dependent on the chemical condition of the ITO electrode, which is affected, at least in part, by the particular method used to clean the ITO prior to device fabrication. Therefore, various TCOs, such as ZnO based TCO or conducting polymer, nanometal, and carbon nanotube, etc. have been investigated and can be applied in OLEDs and/or other optoelectronic devices. For example, ZnO has the advantages, such as the absence of toxicity, low cost, and good thermal stability. ZnO films with a hexagonal wurtzite structure have a wide optical energy band gap (around 3.3 eV). However, the electrical properties of undoped ZnO films are subjected to stoichiometric deviations resulting from oxygen vacancies and interstitial zinc atoms. In order to improve this deficiency, many workers have researched how the electrical properties of future TCO films are influenced by doping or new material development.

4. Acknowledgment

This research was financially supported by the Second Stage of Brain Korea 21 Project and the Ministry of Knowledge Economy(MKE), Korea Institute for Advancement of Technology(KIAT) and Dae-Gyeong Leading Industry Office through the Leading Industry Development for Economic Region.

5. Reference

Agura, H.; Suzuki, H.; Matsushita, T.; Aoki, T. & Okuda, M. (2003). Low Resistivity Transparent Conducting Al-doped ZnO Films Prepared by Pulsed Laser

- Deposition. *Thin Solid Films*, Vol.445, No.2, (December 2003), pp. 263-267, ISSN 0040-6090
- Banerjee, A.N. & Chattopadhyay, K.K. (2005). Recent Developments in The Emerging Field of Crystalline p-Type Transparent Conducting Oxide Thin Films. *Progress in Crystal Growth and Characterization of Materials*, Vol.50, No.3, (September 2005), pp. 55-105, ISSN 0960-8974
- Carter, S. A.; Angelopoulos, M.; Karg, S.; Brock, P. J. & Scott, J. C. (1997). Polymeric Anodes for Improved Polymer Light-Emitting Diode Performance, *Applied Physics Letters*, Vol.70, No.1, (April 1997), pp. 2067-2069, ISSN 0003-6951
- Chan, I. M. & Hong, F. C. (2004). Improved Performance of The Single-Layer and Double-Layer Organic Light Emitting Diodes by Nickel Oxide Coated Indium Tin Oxide Anode. *Thin Solid Films*, Vol.450, No.2, (October 17 2003), pp. 304-311, ISSN 0040-6090
- Chen, M.; Pei, Z.; C, Sun.; L.S, Wen. & X, Wang. (2000). Surface Characterization of Transparent Conductive Oxide Al-Doped ZnO Flms. *Journal of Crystal Growth*, Vol.220, No.3, (February 2000), pp. 254-262, ISSN 0022-0248
- Chen, T. H.; Liou, Y.; Wu, T. J. & Chen, J. Y. (2004). Enhancement of Organic Light-Emitting Device Performances with Hf-Doped Indium Tin Oxide Anodes. *Applied Physics Letters*, Vol.85, No.11, (April 2004), pp. 2092-2094, ISSN 1077-3118
- Chen, Z.; Cotterell, Brian. & Wang, Wei. (2002). The Fracture of Brittle Thin Films on Compliant Substrate in Flexible Displays. *Engineering Fracture Mechanics*, Vol.69, No.5, (February 2002), pp.597-603, ISSN 0013-7944
- Cho, M.-H.; Chang, H. S.; Cho, Y. J.; Moon, D. W.; Min, K.-H.; Sinclair, R.; Kang, S. K.; Ko, D.-H.; Lee, J. H.; Gu, J. H. & Lee, N. I. (2004). Change in Chemical State and Thermal Stability of HfO₂ by The Incorporation of Al₂O₃. *Applied Physics Letters*, Vol.84, No.4, (May 2003), pp. 571-573, ISSN 1077-3118
- Choi, B.G.; Kim, I. H.; Kim, D.H.; Lee, K.S.; Lee. T.S.; Cheong, B.; Baik, Y.-J. & Kim, W.M. (2005) Electrical, Optical and Structural Properties of Transparent and Conducting ZnO Thin Films Doped with Al and F by Rf Magnetron Sputter. *Journal of The European Ceramic Society*, Vol.25, No.12, (March 2005), pp. 2161-2165, ISSN 0955-2219
- Choi, K.; Kim, J.; Lee, Y. & Kim, H. (1999). ITO/Ag/ITO Multilayer Films for The Application of A Very Low Resistance Transparent Electrode. *Thin Solid Films*, Vol.341, No.1-2, (March 1999), pp. 152-155, ISSN 0040-6090
- Chowdhury, F.-U.-Z. & Bhuiyan, A.H. (2000). An Investigation of The Optical Properties of Plasma-Polymerized Diphenyl Thin Films. *Thin Solid Films*, Vol.360, No.1-2, (February 2000), pp. 69-74, ISSN 0040-6090
- Chung, J.-L.; Chen, J.-C. & Tseng, C.-J. (2008). Preparation of TiO₂-Doped ZnO Films by Radio Frequency Magnetron Sputtering in Ambient Hydrogen-Argon Gas. *Applied Surface Science*, Vol.255, No.5, (July 2008), pp. 2494-2499, ISSN 0169-4332
- Custaffson, G.; Treacy, G. M.; Klavertter, Y. C.; Colaneri, N. & Heeger, A. J. (2003). The "Plastic" Led: A Flexible Light-Emitting Device Using A Polyaniline Transparent Electrode. *Synthetic Metals*, Vol.57, No.1, (February 2000), pp. 4123-4127, ISSN 0379-6779
- David, O.; Scanlon, Aron, W. & Graeme, W. W. (2009). Understanding the p-Type Conduction Properties of the Transparent Conducting Oxide CuBO₂: A Density

- Functional Theory Analysis. *Chemistry of Materials*, Vol.21, No.19, (July 2009), pp. 4568–4576, ISSN 0897-4756
- Deng, Z.B.; Ding, X.M. & Lee, S.T. (1999). Enhanced Brightness and Efficiency in Organic Electroluminescent Devices using SiO₂ Buffer Layers. *Applied Physics Letters*, Vol.74, No.15, (December 1998), pp. 2227-2229, ISSN 0003-6951
- Dingle, R.; Störmer, H.-L.; Gossard, A.C. & Wiegmann, W. (1978). Electron Mobilities in Modulation-Doped Semiconductor Heterojunction Superlattices. *Applied Physics Letters*, Vol.33, No.7, (July 1978), pp.665-667, ISSN 0003-6951
- Ghosh, C. K.; Popuri, S. R.; Mahesh, T. U. & Chattopadhyay, K. K. (2006). Preparation of Nanocrystalline CuAlO₂ through Sol-Gel Route. *Journal of Sol-Gel Science and Technology*, Vol.52, No.1 (March 2009), pp. 75-81, ISBN 0928-0707
- Gu, G.; Bulović, V.; Burrows, P. E. & Forrest, S. R. (1996). Transparent Organic Light Emitting Devices. *Applied Physics Letters*, Vol.68, (March 1996), pp. 2606-2608, ISSN 0003-6951
- Guan, H.-S.; Gheng, C.-H.; Li, W.-C.; Geng, D.-F.; Fan, Z.-Q.; Chang, Y. C.; Zhao, W.; Guo, Z.-Q. & Du, G.-T. (2009). Influence of Transparent Anode on Luminescent Performance of Near-Infrared Organic Light-Emitting Diodes. *Chemical Research in Chinese Universities*, Vol.25, No.6, (November 2009), pp. 786-789, ISSN 1005-9040
- Guillen, G. & Herrero, J. (2009). Transparent Conductive ITO/Ag/ITO Multilayer Electrodes Deposited by Sputtering at Room Temperature, *Optics Communications*, Vol.282, No.4, (November 2008), pp. 574-578, ISSN 0030-4018
- Gu, G.; Burrows, P. E.; Forrest, S. R. & Thompson, M. E. (1997). Vacuum-Deposited, Nonpolymeric Flexible Organic Light-Emitting Devices. *Optics Letters*, Vol.22, No.3, (1997), pp. 172-174, ISSN 0146-9592
- Guo, Z.G.; Zhou, F.; Hao, J.C. & Liu, W.M. (2005). Stable Biomimetic Super-Hydrophobic Engineering Materials. *Journal of the American Chemical Society*, Vol.127, No.45, (July 2005), pp. 15670-15671, ISSN 0002-7863
- Han, J.; Mantas, P.Q. & Senos, A.M.R. (2001). Effect of Al and Mn Doping on the Electrical Conductivity of ZnO. *Journal of European Ceramic Society*, Vol.21, No.10-11, (2001), pp. 1883~1886, ISSN 0955-2219
- He, T. & Kanicki, J. (2000). High-Efficiency Organic Polymer Light-Emitting Heterostructure Devices on Flexible Plastic Substrates. *Applied Physics Letters*, Vol.76, No.6, pp. 661-663, ISSN 0003-6951
- Hirata, G.A.; McKittrick, J.; Cheeks, T.; Siqueiros, J.M.; Diaz, J.A.; Contreras, O. & Lopez, O.A. (1996). Synthesis and Optoelectronic Characterization of Gallium Doped Zinc Oxide Transparent Electrodes. *Thin Solid Films*, Vol.288, No.1-2, (November 1996), pp. 29-31, ISSN 0040-6090
- Honda, S.; Tsujimoto, A.; Watamori, M. & Oura, K. (1995). Oxygen Content of Indium Tin Oxide Films Fabricated by Reactive Sputtering. *Journal of Vacuum Science & Technology A: Vacuum, Surfaces, and Films*, Vol.13, No.3, (May 1995), pp. 1100-1103, ISSN 0734-2101
- Huang, C. J. (2003). Silicon Dioxide Buffer at Anode/Polymer Interface for Enhanced Brightness and Efficiency of Polymer Light-Emitting Diode. *Journal of Materials Science Letters*, Vol.22, No.20, (May 2003) pp. 1423-1425 ISSN 1573-4811
- Huang, Y.-J.; Liu, C.-W.; Chu, S.-Y. & Lo, K.-Y. (2010) The Formation of p-Type ZnO Films by Thermal Diffusion from the Low Energy, High Dose Phosphorus-Implanted Si

- Substrate. *Journal of The Electrochemical Society*, Vol.157, No.4, (December 2009), pp. H435-H437, ISBN 0013-4651
- Ishii, H.; Sugiyama, K.; Ito, E. & Seki, K. (1999). Energy Level Alignment and interfacial Electronic Structure at Organic/Metal and Organic/Organic Interfaces. *Advanced Materials*, Vol.11, No.11, (June 1999), pp. 605-625, ISSN 1521-4095
- Kawazoe, H.; Yasukawa, M.; Hyodo, H.; Kurita, M.; Yanagi, H. & Hosono, H. (1997). p-Type Electrical Conduction in Transparent Thin Films of CuAlO_2 . *Nature*, Vol.389, No.6654, (June 1997), pp. 939-942, ISBN 0028-0836
- Kim, H.-M.; Bae, K. & Sohn S. (2011). Electronic and Optical Properties of Indium Zinc Oxide Thin Films Prepared by Using Nanopowder Target. *Japanese Journal of Applied Physics*, Vol.50, No.4, (June 2010), pp. 045801-045805, ISBN 0021-4922
- Kim, H. & Sohn, S. (2009). Preparation of SiO_x and SiO_xN_y Films on PEN using Facing Target Sputtering System. *ECS Transactions*, Vol.19, No.9, (May 2009), pp. 9-16, ISSN 1938-6737
- Kim, H.; Gilmore C.; Piqu'e, A.; Horwitz, J.; Mattoussi, H.; Murata, H.; Kafari, Z. & Chrisey, D. (1999). Electrical, Optical, and Structural Properties of Indium-Tin-Oxide Thin Films for Organic Light-Emitting Devices. *Journal of Applied Physics*, Vol.86, No.11, (June 1999), pp. 6451-6461, ISSN 0021-8979
- Kim, H.; Gilmore, C.; Horwitz, J.; Piqu'e, A.; Murata, H.; Kushto, G.; Schlaf, R.; Kafafi, Z. & Chrisey, D. (2000). Transparent Conducting Aluminum-Doped Zinc Oxide Thin Films for Organic Light-Emitting Devices. *Applied Physics Letters*, Vol.76, No.3, (January 2000), pp. 259-261, ISSN 0003-6951
- Kim, H.; Horwitz, J.S.; Kim, W.H.; Qadri, S.B. & Kafafi, Z.H. (2003). Anode Material Based on Zr-Doped ZnO Thin Films for Organic Light-Emitting Diodes. *Applied Physics Letters*, Vol.83, No.18, (September 2003), pp. 3809-3811, ISSN 0003-6951
- Kim, H.; Kim, H.; Lee, J.; Lee, K.; Yi, J.; Oh, S.; Sohn, S.; Jung, D.; Jang, S. & Chae, H. (2008). Admittance spectroscopic analysis of organic light emitting diodes with the CF_x plasma treatment on the surface of indium tin oxide anodes. *Thin Solid Films*, Vol.516, No.7, (August 2008) pp.1370, ISSN 0040-6090
- Kim, K. H.; Son, I. H.; Song, K. B.; Kong, S. H.; Keum, M. J.; Nakagawa, S. & Naoe, M. (2001). Thin Film Properties by Facing Targets Sputtering System. *Applied surface Science*, Vol.169-170, No.1, (January 2001), pp. 410-414, ISSN 0169-4332
- Kim, S. Y. & Lee, J.-L. (2005). Effect of Thin Iridium Oxide on The Formation of Interface Dipole in Organic Light-Emitting Diodes. *Applied Physics Letters*, Vol.87, No.23, (September 2005), pp. 232105-232107, ISSN 1077-3118
- Kim, Y.; Park, J.; Choi, D.; Jang, H.; Lee, J.; Park, H.; Choi, J.; Ju, D.; Lee, J. & Kim, D. (2007). ITO/Au/ITO Multilayer Thin Films for Transparent Conducting Electrode Applications. *Applied Surface Science*, Vol.254, No.5, (June 2007), pp. 1524-1527, ISSN 0169-4332
- Kudo, A.; Yanagi, H.; Hosono, H. & Kawazo, H. (1998). SrCu_2O_2 : A p-Type Conductive Oxide with Wide Band Gap. *Applied Physics Letters*, Vol. 73, (May 1998), pp. 220-222, ISSN 0003-6951
- Kwon, S. H.; Paik, S. Y. & Yoo, J. S. (2002). Electroluminescent Properties of MEH-PPV Light-Emitting Diodes Fabricated on The Flexible Substrate. *Synthetic Metals*, Vol.130, No.1, (August 2002), pp. 55-60, ISSN 0379-6779

- Li, C.; Furuta, M.; Hiramatsu, T.; Furuta, H. & Hirao, T. (2009). Effects of Substrate on The Structural, Electrical and Optical Properties of Al-Doped ZnO Films Prepared by Radio Frequency Magnetron Sputtering. *Thin Solid Films*, Vol.517, No.11, (November 2008), pp. 3265-3268, ISSN 0400-6090
- Li, J.; Yahiro, M.; Ishida, K.; Yamada, H. & Matsushige K. (2005). Enhanced Performance of Organic Light Emitting Device by Insertion of Conducting/Insulating WO₃ Anodic Buffer Layer. *Synthetic Metals*, Vol.151, No.2, (May 2005), pp. 141-146, ISSN 0379-6779
- Lu, H. T. & Yokoyama, M. (2003). Enhanced Emission in Organic Light-Emitting Diodes using Ta₂O₅ Buffer layers. *Solid-State Electronics*, Vol.47, No.8, (December 2002), pp. 1409-1412, ISSN 0038-1101
- Mardare, D.; Tascu, M.; Delibas, M. & Rusu, G.I. (2000). On The Structural Properties and Optical Transmittance of TiO₂ R.F. Sputtered Thin Films. *Applied surface Science*, Vol.156, No.1-4, (2000), pp. 200-206, ISSN 0169-4332
- Medvedeva, J. E. (2006). Magnetically Mediated Transparent Conductors: In₂O₃ Doped with Mo. *Physical Review Letters*, Vol.97, No.8, (August 2006), pp. 086401-086404, ISSN 0031-9007
- Minami T.; Nanto, H. & Takata, S. (1985). Highly Conductive and Transparent Aluminum Doped Zinc Oxide Thin Films Prepared by RF Magnetron Sputtering. *Thin Solid Films*, Vol.124, No.1, (February 1985), pp. 43-47, ISSN 0040-6090
- Minami, T. (1999) Transparent and conductive multicomponent oxide films prepared by magnetron sputtering. *Journal of Vacuum Science & Technology A: Vacuum, Surfaces, and Films*, Vol.17, No.4, (July 1999), pp. 1765-1772, ISSN 0734-2101
- Mitsui, A. & Masumo, K. (2003). Effect of Zirconium Oxide Undercoat on Microstructure and Properties of Tin-Doped Indium Oxide Film for Organic Light Emitting Devices. *Thin Solid Films*, Vol. 442, No.1-2, (September 2003), pp. 140-144, ISSN 0040-6090
- Miyata, T.; Minami, T.; Shimokawa, K.; Kakumu, T. & Ishii, M. (1997). New Materials Consisting of Multicomponent Oxides for Thin-Film Gas Sensors, *Journal of the Electrochemical Society*, Vol.144, No.7, (February 1997), pp. 2432-2436, ISSN 0013-4651
- Nose, M.; Nagae, T.; Yokota, M.; Saji, S.; Zhou, M. & Nakada, M. (1999). Electrical and Colorimetric Properties of TiN Thin Films Prepared by DC Reactive Sputtering in a Facing Targets Sputtering (FTS) System. *Surface and Coatings Technology*, Vol.116-119, No.1, (September 1999), pp. 296-301, ISSN 0257-8972
- Ohta, H.; Orita, M.; Hirano, M.; Tanji, H.; Kawazoe, H. & Hosono, H. (2000). Highly Electrically Conductive Indium-Tin-Oxide Thin Films Epitaxially Grown on Yttria-Stabilized Zirconia(100) by Pulsed-Laser Deposition. *Applied Physics Letters*, Vol.76, No.19, (March 2000), pp. 2740-2742, ISBN 0003-6951
- Ott, A.W. & Chang, R.P.H. (1999). Atomic Layer-Controlled Growth of Transparent Conducting ZnO on Plastic Substrates. *Materials Chemistry and Physics*, Vol.58, No.2, (November 1998), pp. 132-138, ISSN 0254-0584
- Park, J.-M.; Hong, J.-S.; Kim, J.-J.; Park, S.-H.; Kim, H.-M. & Ahn, J.-S. (2006). Bending Effects of Indium-Zinc Oxide Thin Films Deposited on Polyethylene Terephthalate Substrate by Radio Frequency Magnetron Sputtering. *Journal of the Korean Physical Society*, Vol.48, No.6, (June 2006), pp.1530-1533, ISSN 0374-4884

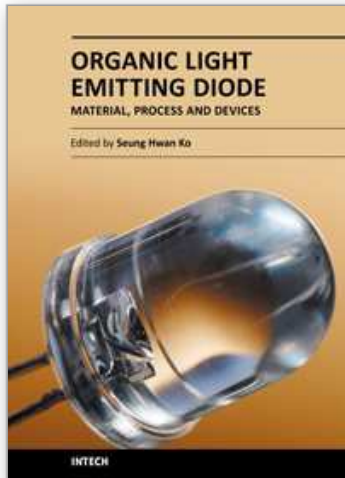
- Park, J. H.; Cho, Y. C.; Shin, J. M.; Cha, S.-Y.; Cho, C. R.; Kim, H. S.; Yoon, S. J.; Jeong, S.-Y.; Park, S. E.; & Lim, A.-R. (2007). A Study of Transparent Conductive Aluminum-Doped Zinc Oxide Fabricated on a Flexible Polyethersulphone (PES) Substrate. *Journal of the Korean Physical Society*, Vol.51, No.6 (December 2007), pp. 1968-1972, ISSN 0374-4884
- Park, J. M.; Kim, J. J.; Kim, H. M.; Kim, J. H.; Ryu, S. W.; Park, S. H. & Ahn, J. S. (2006). Substrate Effects on The Characteristics of $(\text{In}_2\text{O}_3)_{1-x}(\text{ZnO})_x$ Films. *Journal of the Korean Physical Society*, Vol.48, No.6, (June 2006), pp. 1624-1627, ISSN 0374-4884
- Park, S.-M.; Ikegami, T. & Ebihara, K. (2006). Effects of Substrate Temperature on the Properties of Ga-doped ZnO by Pulsed Laser Deposition. *Thin Solid Films*, Vol.513, No.1-2, (December 2005), pp. 90-94, ISSN 0040-6090
- Qiu, C.; Xie, Z.; Chen, H; Wong, M. & Kwok, H. S. (2003). Comparative Study of Metal or Oxide Capped Indium Tin Oxide Anodes for Organic Light-Emitting Diodes. *Journal of Applied Physics*, Vol.93, No.6, (January 6 2003), pp. 3253-3258, ISSN 1089-7550
- Rauf, I.A. (1993). Low Resistivity and High Mobility Tin-Doped Indium Oxide Films. *Materials Letters*, Vol.18, No.3, (September 1993), pp. 123-127, ISSN 0167-577X
- Robins, J. J. & Wolden, C.A. (2003). High Mobility Oxides: Engineered Structures to Overcome Intrinsic Performance Limitations of Transparent Conducting Oxides. *Applied Physics Letters*, Vol.83, No.19, (September 2003), pp. 3933-3935, ISSN 0003-6951
- Roy, B.; Ode, A.; Readey, D.; Perkins, J.; Parilla, P. Tepliin, C.; Kaydanova, T.; Miedaner, A.; Curtis, C.; Martinson, A.; Coutts, T.; Ginley, D. & Hosono, H. (2003). Towards High Performance p-Type Transparent Conducting Oxides. *National Center for Photovoltaics and Solar Program Review Meeting*, Denver, Colorado, March 24-26, 2003, NREL reported NREL/CP-520-33595
- Sato, H.; Minami, T.; Takata, S. & Yamada, T. (2003). Transparent Conducting p-Type NiO Thin Films Prepared by Magnetron Sputtering. *Thin Solid Films*, Vol. 236, No. 1-2, (December 1993), pp. 27-31, ISSN 0040-6090
- Shan, F.K.; Shin, B.C.; Kim, S.C. & Yu, Y.S. (2003). Optical Property and Aging Effect of ZnO Thin Films. *Journal of the Korean Physical Society*, Vol.42, No.94, (April 2003), pp. S1174-1177, ISSN 0374-4884
- Sheng, S.; Fang, G.; Li, C.; Xu, S. & Zhao, X. (2006). p-Type Transparent Conducting Oxides. *Physica Status Solidi (a)*, Vol.203, No.8, (April 2006), pp. 1891-1900, ISSN1862-6300
- Shrotriya, V. & Yang, Y. (2005). Capacitance-Voltage Characterization of Polymer Light-Emitting Diodes. *Journal of Applied Physics*, Vol.97, No.5, (December 2004), pp. 54504-54509, ISSN 1089-7550
- Snure, M. & Tiwari, A. (2007). CuBO_2 : A p-Type Transparent Oxide. *Applied Physics Letter*, Vol.91, No.9, (July 2007), pp. 092123-092125, ISBN 0003-6951
- Sohn, S.; Lee, J.; Park, K.; Jung, D.; Kim, H. & Yi, J. (2008). Enhanced Performance of an Organic Light-Emitting Device by Using an Oxidant Component during a Surface Reaction Process by Using Atomic Layer Chemical Vapor Deposition. *Journal of the Korean Physical Society*, Vol. 53, No.6, (June 2008), pp. 3416-3421, ISSN 0374-4884
- Takiji, S.; Kohei, I. & Seimei, S. (2004). Ultra-water-repellent surface: fabrication of complicated structure of SiO_2 nanoparticles by electrostatic self-assembled films.

- Applied Surface Science*, Vol.237, No.3, (September 2004), pp. 539-543, ISSN 0169-4332
- Teplin, C.; Kaydanova, T.; Young, D.; Perkins, J. & Ginley, D. (2004), A Simple Method for the Preparation of Transparent p-Type Ca-doped CuInO_2 Films: Pulsed-Laser Deposition from Air-Sintered Ca-Doped $\text{Cu}_2\text{In}_2\text{O}_5$ Targets. *Applied Physics Letters*. Vol.85, No.17, (October 2004), pp. 3789-3791, ISSN 0003-6951
- Tuttle, G.; Kroemer, H. & English, J. H. (1989). Electron Concentrations and Mobilities in AlSb/InAs/AlSb Quantum Wells. *Journal of Applied Physics*, Vol.65, No.12, (February 1989), pp. 5239-5242, ISSN 0021-8979
- Ueda, K.; Tabata, H. & Kawai, T. (2001). Magnetic and Electric Properties of Transition-Metal-Doped ZnO Films. *Journal of Applied Physics*, Vol.79, No.7, (August 2001), pp. 988-990, ISSN 0021-8979
- Ueda, K.; Hase, T.; Yanagi, H.; Kawazoe, H.; Hosono, H.; Ohta, H.; Orita, M. & Hirano, M. (2001). Epitaxial Growth of Transparent p-Type Conducting CuGaO_2 Thin Films on Sapphire (001) Substrates by Pulsed Laser Deposition. *Journal of Applied Physics*, Vol.89, No.3, pp. (July 2000), pp. 1790-1793, ISSN 1089-7550
- VanSlyke, S. A.; Chen, C. H. & Tang, C. W. (1996). Organic Electroluminescent Devices with Improved Stability. *Applied Physics Letters*, Vol.69, No.15, (August 1996), pp. 2160-2162, ISSN 1077-3118
- Wang, R.-C.; Liu, C.-P.; Huang, J.-L. & Chen, S.-J. (2006). Single-Crystalline AlZnO Nanowires/Nanotubes Synthesized at Low Temperature. *Applied Physics Letters*. Vol.88, No.2, (August 2005), pp. 023111-023113, ISSN 0003-6951
- Yan, Y.; S.J, P.; Dai, J.; Chang, R.P.H.; Wang, A. & Marks, T.J., (1998). Polytypoid Structures in Annealed In_2O_3 - ZnO Films, *Applied Physics Letters*, Vol.73, No.18, (August 1998), pp. 2585-2587, ISSN 0003-6951
- Yanagi, H.; Hase, T.; Ibuki, S.; Ueda, K. & Hosono, H. (2000). Bipolarity in Electrical Conduction of Transparent Oxide Semiconductor CuInO_2 with Delafossite Structure. *Applied Physics Letters*, Vol.78, No.11, (January 2001), pp. 1583-1585, ISSN 0003-6951
- Yanagi, H.; Kawazoe, H.; Kudo, A.; Yasukawa, M. & Hosono, H. (2000). Chemical Design and Thin Film Preparation of p-Type Conductive Transparent Oxides. *Journal of Electroceramics*, Vol. 4, (June 2000), pp. 407-414, ISSN 1385-3449
- Yanagi, H.; Ueda, K.; Ohta, H.; Orita, M, Hirano, M. & Hosono, H. (2002). Fabrication of All Oxide Transparent p-n Homojunction using Bipolar CuInO_2 Semiconducting Oxide with Delafossite Structure. *Solid State Communication*, Vol.121, No.1, (December 2001), pp. 15-17, ISSN 0038-1098
- Yang, M.; Xiliang, Y.; Huaxian, C.; Jie, S.; Yiming, J.; Zhuangjian, Z. & Zhongyi, H. (2001). A New Transparent Conductive Thin Film In_2O_3 :Mo. *Thin Solid Films*, Vol. 394, No.2, (August 2001), pp. 219-223, ISSN 0040-6090
- Yang, T.L.; Zhang, D.H.; Ma, J.; Ma, H.L. & Chen, Y. (1998). Transparent Conducting ZnO:Al Films Deposited on Organic Substrates Deposited by R.F. Magnetron-Sputtering. *Thin Solid Films*, Vol.326, No.1, (August 1998), pp. 60-62, ISSN 0040-6090
- Yoshida, Y.; Wood, D. M.; Gessert, T. A. & Coutts, T. J. (2004). High-Mobility Sputtered Films of Indium Oxide Doped with Molybdenum. *Applied Physics Letters*. Vol.84, No.12, (January 2004), pp. 2097-2099, ISSN 0003-6951

Zhang, Y. & Forrest, S. R. (1993). Mechanisms of Quasiepitaxial Ordering at Molecular Thin Film Interfaces. *Physical Review Letters*, Vol.71, No.17, (October 1993), pp. 2765-2768, ISSN 0031-9007

IntechOpen

IntechOpen



Organic Light Emitting Diode - Material, Process and Devices

Edited by Prof. Seung Hwan Ko

ISBN 978-953-307-273-9

Hard cover, 322 pages

Publisher InTech

Published online 27, July, 2011

Published in print edition July, 2011

This book contains a collection of latest research developments on Organic light emitting diodes (OLED). It is a promising new research area that has received a lot of attention in recent years. Here you will find interesting reports on cutting-edge science and technology related to materials, fabrication processes, and real device applications of OLEDs. I hope that the book will lead to systematization of OLED study, creation of new research field and further promotion of OLED technology for the bright future of our society.

How to reference

In order to correctly reference this scholarly work, feel free to copy and paste the following:

Sunyoung Sohn and Yoon Soo Han (2011). Transparent Conductive Oxide (TCO) Films for Organic Light Emissive Devices (OLEDs), Organic Light Emitting Diode - Material, Process and Devices, Prof. Seung Hwan Ko (Ed.), ISBN: 978-953-307-273-9, InTech, Available from: <http://www.intechopen.com/books/organic-light-emitting-diode-material-process-and-devices/transparent-conductive-oxide-tco-films-for-organic-light-emissive-devices-oleds->

INTECH
open science | open minds

InTech Europe

University Campus STeP Ri
Slavka Krautzeka 83/A
51000 Rijeka, Croatia
Phone: +385 (51) 770 447
Fax: +385 (51) 686 166
www.intechopen.com

InTech China

Unit 405, Office Block, Hotel Equatorial Shanghai
No.65, Yan An Road (West), Shanghai, 200040, China
中国上海市延安西路65号上海国际贵都大饭店办公楼405单元
Phone: +86-21-62489820
Fax: +86-21-62489821

© 2011 The Author(s). Licensee IntechOpen. This chapter is distributed under the terms of the [Creative Commons Attribution-NonCommercial-ShareAlike-3.0 License](#), which permits use, distribution and reproduction for non-commercial purposes, provided the original is properly cited and derivative works building on this content are distributed under the same license.

IntechOpen

IntechOpen